

For Reference

NOT TO BE TAKEN FROM THIS ROOM

Ex LIBRIS
UNIVERSITATIS
ALBERTAEISIS



T H E U N I V E R S I T Y O F A L B E R T A

RELEASE FORM

NAME OF AUTHOR Stephen Andrew McQuarrie

TITLE OF THESIS THE PRODUCTION OF POSITRON EMITTING
 NUCLIDES BY A VAN DE GRAAFF FOR
 USE IN NUCLEAR MEDICINE

DEGREE FOR WHICH THESIS WAS PRESENTED: MASTER OF SCIENCE

YEAR THIS DEGREE GRANTED: 1975

Permission is hereby granted to THE UNIVERSITY OF
ALBERTA LIBRARY to reproduce single copies of this
thesis and to lend or sell such copies for private,
scholarly or scientific research purposes only.

The author reserves other publication rights, and
neither the thesis nor extensive extracts from it may
be printed or otherwise reproduced without the author's
written permission.

THE UNIVERSITY OF ALBERTA

THE PRODUCTION OF POSITRON-EMITTING NUCLIDES BY A VAN DE GRAAFF
FOR USE IN NUCLEAR MEDICINE

by



STEPHEN ANDREW McQUARRIE

A THESIS

SUBMITTED TO THE FACULTY OF GRADUATE STUDIES AND RESEARCH IN
PARTIAL FULFILMENT OF THE REQUIREMENTS FOR THE DEGREE
OF MASTER OF SCIENCE

DEPARTMENT OF PHYSICS

EDMONTON, ALBERTA

FALL, 1975

THE UNIVERSITY OF ALBERTA
FACULTY OF GRADUATE STUDIES AND RESEARCH

The undersigned certify that they have read, and recommend to the Faculty of Graduate Studies and Research, for acceptance, a thesis entitled THE PRODUCTION OF POSITRON-EMITTING NUCLIDES BY A VAN DE GRAAFF FOR USE IN NUCLEAR MEDICINE submitted by STEPHEN ANDREW McQUARRIE in partial fulfilment of the requirements for the degree of Master of SCIENCE.

ABSTRACT

Alterations and additions were made to the 7 MV Van de Graaff accelerator installation at the University of Alberta to facilitate the production of short-lived positron-emitting nuclides.

To produce sufficient quantities of activity, a new facility was constructed to reduce the prompt neutron radiation generally associated with the production of positron-emitting nuclides. This facility permitted the use of beam currents of as high as $20/\mu\text{A}$.

Two short-lived positron-emitting nuclides were produced: ^{11}C , with a half-life of 20.3 minutes, was produced by the $^{11}\text{B}(\text{p},\text{n})^{11}\text{C}$ reaction, and ^{18}F , with a half-life of 109.8 minutes, was produced by the $^{20}\text{Ne}(\text{d},\alpha)^{18}\text{F}$ reaction.

Carbon-11 labelled CO_2 was produced for use in regional lung function studies. Various methods were evaluated for the collection and purification of $^{11}\text{CO}_2$. The best method combined a copper oxide furnace with a liquid isopentane cold trap.

Fluorine-18 was used to label several precursors of 5-fluoro-2'-deoxyuridine. Five-fluoro-2'-deoxyuridine will be used in diagnostic oncology. Various precursors were tested for uptake of ^{18}F . Maximal uptake was achieved with a solution of potassium fluoride and distilled water which incorporated approximately 70 per cent of the ^{18}F produced.

ACKNOWLEDGEMENTS

I would like to thank my supervisors, Dr. J.M. Cameron and Dr. R.E. Snyder for their advice and encouragement throughout all phases of my work. Dr. Cameron was always available for consultation and took an active part in the experimental portion of the work. His help was invaluable. I am particularly grateful to Dr. Snyder for patiently spending long hours helping me in the preparation of this thesis, and also to Dr. T.R. Overton for his advice during its writing.

Thanks are extended to Dr. L.I. Wiebe and Doug Abrams for providing many detailed explanations regarding the chemistry involved in the ^{18}F -labelled compounds. Without their help and advice this work would not have been possible.

Jock Elliot, Con Green, Henry Nielson, Ernie Pearce and Don Presakarchuk were very cooperative and helpful during my work and I would like to express my gratitude to them.

Many thanks to Trudy Bucharsky for her excellent and expeditious typing of this thesis.

I would also like to thank my wife, Joyce, for her encouragement and support during the past two years. She has been very understanding of the long hours I have spent at my work.

TABLE OF CONTENTS

CHAPTER		PAGE
1	INTRODUCTION	1
1.1	BACKGROUND	1
1.2	PRESENT STUDIES	9
2	THEORY	12
2.1	PRODUCTION OF RADIONUCLIDES	12
2.2	YIELD OF RADIONUCLIDES	23
2.3	POSITRON DECAY	25
3	FACILITY FOR ISOTOPE PRODUCTION	31
3.1	INTRODUCTION	31
3.2	CONSTRUCTION OF THE FACILITY FOR ISOTOPE PRODUCTION	33
3.3	MONITORING OF BEAM CONDITIONS	37
3.4	PROTECTION OF THE VAN DE GRAAFF	43
4	PRODUCTION AND UTILIZATION OF $^{11}\text{CO}_2$	45
4.1	INTRODUCTION	45
4.2	PRODUCTION SYSTEM	47
4.3	ANALYSIS OF $^{11}\text{CO}_2$	51
4.4	UTILIZATION OF $^{11}\text{CO}_2$ IN LUNG FUNCTION STUDIES	53
5	PRODUCTION OF ^{18}F -LABELLED URACIL	62
5.1	INTRODUCTION	62
5.2	PRODUCTION SYSTEM	64
5.3	ANALYSIS OF ^{18}F -LABELLED COMPOUNDS	71
5.4	UTILIZATION OF 5-FLUORO-2'-DEOXYURIDINE IN ONCOLOGY	72

TABLE OF CONTENTS

CHAPTER	PAGE
REFERENCES	75

LIST OF TABLES

TABLE	PAGE
1 A LIST OF SOME POSITRON-EMITTING NUCLIDES THAT MAY BE PRODUCED WITH A 7 MV VAN DE GRAAFF	22

LIST OF FIGURES

FIGURE		PAGE
1	ISORESPONSE CURVES OF A 2.5 cm x 1.27 cm NaI(T1) SCINTILLATION DETECTOR	5
2	EFFECT OF RESONANCE LEVELS ON THE REACTION CROSS SECTION	14
3	TWO-BODY REACTION KINEMATICS	17
4	ACTIVITY GROWTH CURVE	26
5	SCHEMATIC DIAGRAM OF VAN DE GRAAFF	32
6	PHOTOGRAPH OF SHIELDING ENCLOSURE	38
7	FLOOR PLAN OF SHIELDING ENCLOSURE	39
8	SCHEMATIC DIAGRAM OF BASEMENT BEAM-LINE	41
9	CROSS SECTION OF $^{11}\text{B}(\text{p},\text{n})^{11}\text{C}$ REACTION	46
10	^{11}C PRODUCTION SYSTEM	48
11	USE OF A RADIOACTIVE GAS IN REGIONAL LUNG FUNCTION STUDIES	55
12	SCHEMATIC DIAGRAM OF REGIONAL VENTILATION AND PERfusion MEASUREMENTS OF NORMAL AND ABNORMAL LUNG CONDITIONS	57
13	PHOTOGRAPH OF 16-PROBE DETECTION SYSTEM	58
14	SCHEMATIC DIAGRAM OF PHANTOM STUDY	60
15	CROSS SECTION OF $^{20}\text{Ne}(\text{d},\alpha)^{18}\text{F}$ REACTION	63
16	F PRODUCTION SYSTEM	65
17	URACIL LABELLED WITH $^{18}\text{F}_2$ GAS	67
18	URACIL LABELLED WITH LiB $^{18}\text{F}_4$	
19	URACIL LABELLED WITH K ^{18}F	70
20	CHEMICAL STRUCTURE OF 5-FLUORO-2'-DEOXYURIDINE	73

CHAPTER 1

INTRODUCTION

1.1 Background

Nuclear medicine may be defined as that branch of medicine that utilizes nuclear radiation in the diagnosis and treatment of disease. Although its origins are difficult to pinpoint, early landmarks would include the discovery of x-rays by W.K. Roentgen in 1895 and the discovery of radium by M. Curie in 1898. Each of these advances in the physical sciences was followed closely by biological and medical applications. Only months after x-rays were discovered, attempts were made to use them to treat various diseases, including cancer.¹ By 1900, skin lesions were being treated with radium and in 1913, an American physician, R. Abbey, reported the first cure of cancer of the cervix,² which had been treated with radium seven years earlier. However, it was not until the mid 1940's, following the development of the atomic reactor and the cyclotron, that large numbers of radionuclides became available to the medical community and nuclear medicine began to flourish.³

By 1945, more than 375 radionuclides had been produced,⁴ and many proved exceptionally useful in diagnostic nuclear medicine, particularly as tracers in the study of the metabolism of various elements. These radionuclides were initially used *in vitro* ("in glass") in studies designed to determine various properties of samples taken from patients. One of the first tests involved the measurement of red-cell volume⁵ with an isotope of iron, ⁵⁹Fe. The success of *in vitro* studies led to the *in vivo* ("in a living body") use of radionuclides to study biological functions and to detect abnormalities of organs. One

of the initial studies involved the use of ^{131}I to delineate the thyroid, thereby establishing thyroid function.⁶

Early techniques used to visualize the distribution of radio-nuclides within the body involved the use of a hand-held Geiger counter, used to map out the spatial boundaries of the activity. This approach led to the development of a system in which a detector moved mechanically over the region of interest. Known as a rectilinear scanner this device was developed by B. Cassen.⁷ The rectilinear scanner⁸ consists of a radiation detector coupled with a focusing collimator, and electronics to process the information received from the detector. When imaging, the detector scans the distribution of radioactivity in two dimensions. The scanning time for a large organ such as the liver is on the order of forty minutes when operating at relatively fast scanning speeds.

In the early 1960's an important step forward in organ imaging was made by H.O. Anger with the development of a scintillation or gamma camera.⁹⁻¹¹ The scintillation camera produces pictures similar to those of the rectilinear scanner, but in less time due to its higher sensitivity. A typical commercial scintillation camera consists of a 28 cm diameter x 1.3 cm thick NaI(Tl) crystal viewed by a hexagonal array of nineteen photomultiplier tubes, plus the associated electronics for data processing. The position of an incident photon can be determined in two dimensions by the relative amounts of light seen by each photomultiplier tube when a scintillation occurs in the crystal. Utilizing a multihole collimator, the radionuclide distribution may then be determined.

The images produced by the rectilinear scanner and the scintillation camera involve the detection of single photons. To produce an acceptable image, there must be enough activity in the region of interest for the detector to accurately reproduce the distribution. However, when using radionuclides in diagnostic nuclear medicine, it is important to maintain a low radiation dose to the patient. This may be accomplished either by administering low quantities of activity or by using radionuclides with short physical and/or biological half-lives. In general, the administration of low quantities of activity precludes dynamic imaging since long static imaging times are required.

In single photon imaging, the sensitivity, i.e., the ratio of the photons detected to those emitted, is low due to the need for a collimator, which typically allows only 10^{-4} to 10^{-5} of the emitted photons to reach the detector.¹² Using positron-emitting nuclides it is possible to produce an image with a camera that does not need a collimator. This is possible because the emitted positron readily combines with an electron when stopped by matter, whereupon it is annihilated with the conversion of mass energy into two 511-keV gamma rays which travel 180° apart. A pair of detectors, situated on opposite sides of the positron will thus yield the straight line on which the annihilation occurred. Coincidence circuitry is employed to reject spurious data caused by two unrelated gamma rays.

Compared to single photon imaging, the coincidence imaging of positron-emitting nuclides offers high spatial resolution and uniform depth response without the use of collimators. To visualize these

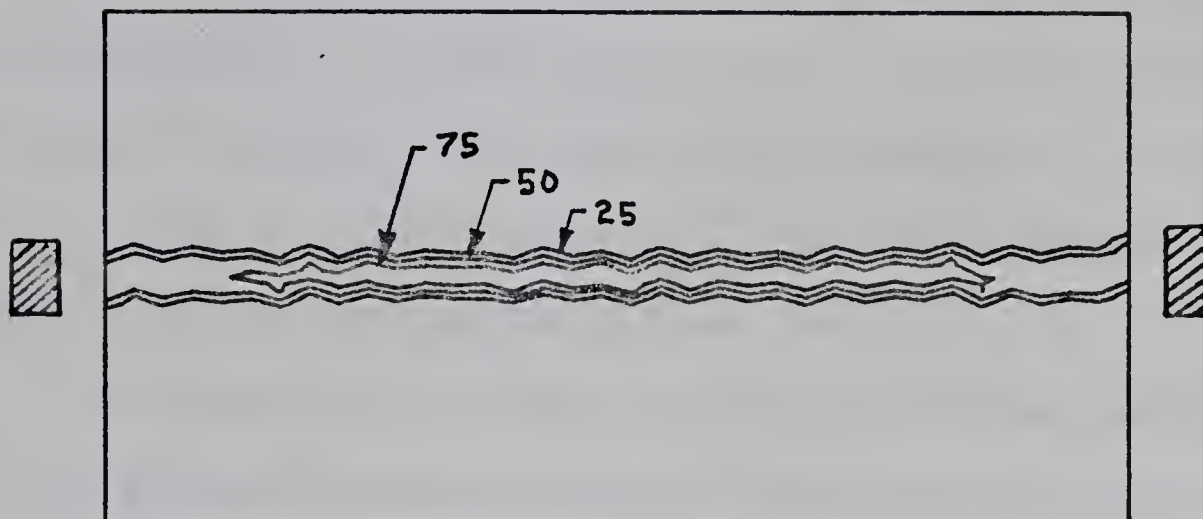
effects, an isoresponse curve has been plotted in Figure 1a for the coincidence detection of a positron-emitting source. As a comparison a second isoresponse curve, Figure 1b, was plotted under the same conditions, except that the detector outputs were summed instead of operated in coincidence. From Figure 1a it can be seen that the region sensitive to positron decay is symmetric and relatively independent of the longitudinal position of the source. If there was an absorber between the detectors, such as tissue, the overall sensitivity would be decreased, but the spatial resolution would remain approximately the same. The longitudinal symmetry of coincidence detection leads to a relatively uniform depth response which is particularly useful when dealing with such problems as the localization of deep lying tumors.

Most positron-emitting nuclides possess short half-lives (<5 hrs.). Although the use of positrons offer many benefits, including lower radiation doses to the patient, and through coincidence detection, the ability to produce images with uniform depth response and high sensitivity, their short half-lives present three disadvantages:

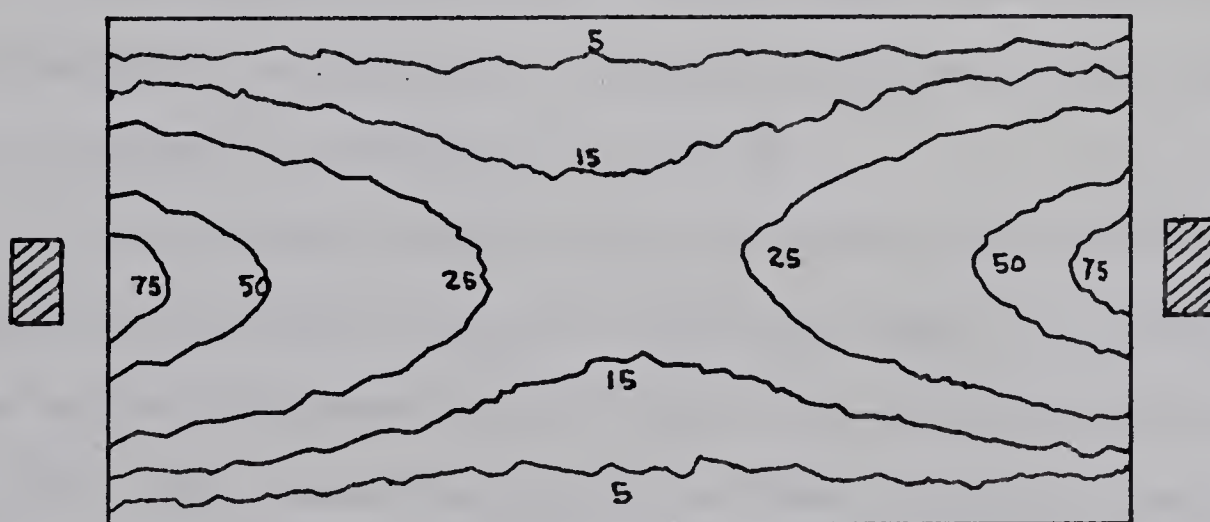
1. they cannot be used as tracers in processes of long duration with respect to the half-life of the radionuclide used,
2. the short-lived radionuclides cannot be incorporated into compounds if the chemical labelling process is long compared to the half-life of the radionuclide, and
3. the short half-lives limit their use to within short distances from their production site.

The use of short-lived radionuclides in medicine is therefore limited to the study of rapidly occurring general dynamic phenomena, or to

ISORESPONSE CURVES OF A
2.54 CM X 1.27 CM NaI(Tl)
SCINTILLATION DETECTOR
(IN AIR)



COINCIDENCE DETECTION



SINGLE PHOTON DETECTION

FIGURE 1

visualize organs which rapidly accumulate the labelled compounds, by means of compounds which can be rapidly synthesized.

The potential usefulness of short-lived positron emitting nuclides in diagnostic nuclear medicine was recognized as early as 1944 when C.A. Tobias and J.H. Lawrence used carbon monoxide, labelled with cyclotron produced ^{11}C , to study the elimination of carbon monoxide from the body.¹³ Another short-lived positron emitter, ^{68}Ga , was used in the early 1950's by F.W. Wren, et al.¹⁴ and by G.C. Brownell and W.H. Sweet¹⁵ for the localization of brain tumors.

Early imaging of positron-emitting nuclides was performed either by treating the radionuclide as a single photon emitter or by employing two opposed detectors operating in coincidence. In an effort to combine the advantages of coincidence techniques with those of the gamma camera,¹⁶ H.O. Anger developed a "positron camera" which consists of a normal gamma camera combined through coincidence logic to a second gamma camera head. The camera is capable of producing tomographic images with a spatial resolution of 8-10 mm, high sensitivity and a uniform depth of field response. A detailed discussion of the positron camera is presented in references 17 and 18.

Several other positron detection systems have evolved in the last ten years for use in diagnostic medicine, among them a multi-detector system, the Massachusetts General Hospital (MGH) positron camera.^{19,20} This camera consists of two fixed identical planar arrays, each containing 127 small NaI(Tl) crystals viewed by an array of 72 photomultiplier tubes. This design achieves a count-rate capability of 5×10^4 coincidence events per second, a field of view of approximately 27 cm x 30 cm and a spatial resolution of less than one centimeter at

midplane. As well as being a medical research tool, the MGH camera is routinely used for brain tumor localization and the measurement of regional lung ventilation and perfusion.

Recently, considerable attention has been given to the possibility of three-dimensional image reconstruction. In the EMI-scanner,^{21,22} a large number of x-ray absorption measurements are made along different paths through the brain. Using a small digital computer, it is possible to obtain approximate solutions to a system of simultaneous equations and thus obtain the absorption coefficient at any point within the brain. These techniques, applied initially to radiology, have now been extended into nuclear medicine. Various groups^{23,24} have produced algorithms and modified single photon systems for the reconstruction of three-dimensional images. Once again however, the use of positrons may offer benefits over single photon imaging due to improvements in sensitivity and uniformity of response. Work is already underway on this topic.²⁵⁻²⁷

The production of radionuclides is possible through nuclear reactions induced by nuclear reactors or accelerators, or through the decay of long-lived radionuclides. If the desired radionuclide is generated from the decay of a longer-lived radionuclide, then the shorter-lived daughter may be chemically separated from the longer-lived parent.^{28,29} The production of short-lived radionuclides by radionuclide generators is particularly useful in medical applications because it requires only a modest outlay of apparatus and provides an economical source of radionuclides for the clinical laboratory. Several short-lived radionuclides useful for diagnostic purposes may be prepared

in this manner, including the short-lived positron emitter ^{68}Ga . However, at present, this method provides only a small number of medically useful short-lived radionuclides: most are produced through nuclear reactions.

The majority of medically useful positron-emitting nuclides that are prepared by nuclear reactions are most easily produced by means of a particle accelerator. At present, the cyclotron appears to be best suited for this purpose. The cyclotron, as were other types of particle accelerators, was initially developed for the investigation of nuclear structure, and since this machine and its associated facilities are rather large and complex, its use has been limited largely to the fundamental nuclear sciences. However, since conception of the cyclotron, the radionuclides produced by them have been of interest to biomedical research. Several recent international conferences have been devoted to the subject of the use of cyclotrons for research in other disciplines, including medicine.³⁰

The recent development of small compact cyclotrons³¹ has enabled installation of such devices in medical institutions dedicated solely to biomedical applications. These compact cyclotrons are capable of producing a number of short-lived radionuclides of particular interest to biological and medical applications.³² The applications of cyclotrons to medicine and medical cyclotron facilities that are presently or soon will be in operation have been reviewed by H.I. Glass and D.J. Silvester.³³

The Van de Graaff accelerator has also been used to generate a number of short-lived radionuclides. Although this type of machine is generally limited to operating at accelerating potentials less than 10 MV

and with external beam currents of less than 30 μA ,³⁴ a number of short-lived radionuclides have been produced in sufficient quantities for use in diagnostic nuclear medicine.^{35,36} The restriction in the incident beam energy precludes the use of a Van de Graaff to produce useable quantities of the heavier radionuclides due to Coulomb barrier effects. However, several short-lived positron-emitting nuclides of biological and medical interest, ^{11}C , ^{13}N , ^{15}O and ^{18}F are readily produced in sufficient quantities by Van de Graaff machines operating in the range of 6-10 MV. The topic of this thesis is concerned with the use of a 7 MV Van de Graaff accelerator in the production of short-lived positron-emitting nuclides.

1.2 Present Studies

The 7 MV Van de Graaff accelerator at the University of Alberta, although primarily used for the investigation of nuclear structure, was used to produce positron-emitting nuclides for medical use. This work was partially initiated in response to other groups at the University of Alberta which were interested in undertaking medical studies using positron emitters and possessed the necessary instrumentation to utilize such radionuclides.

The Van de Graaff and its associated accelerator facilities were developed primarily for use in the study of nuclear science, and hence, several modifications were necessary in order that usable quantities of positron-emitting nuclides could be safely produced. The necessary modifications to the accelerator consisted of:

1. increasing the available beam current to raise the yield of the radionuclides, and

2. providing adequate shielding to reduce the high neutron radiation generally associated with the production of positron-emitting nuclides.

These modifications were incorporated into a new facility built for the purpose of producing positron-emitting nuclides for use in diagnostic nuclear medicine. This aspect of the thesis will be discussed in Chapter 3.

Although the primary interest was in any positron-emitting nuclide producible with the Van de Graaff, two were chosen for specific studies: ^{11}C , with a half-life of 20.3 min., produced by the $^{11}\text{B}(\text{p},\text{n})^{11}\text{C}$ reaction and ^{18}F , with a half-life of 109.7 min., produced by the $^{20}\text{Ne}^{20}\text{Ne}(\text{d},\alpha)^{18}\text{F}$.

The impetus for producing ^{11}C was through the affiliation between the Department of Physics and the Division of Biomedical Engineering. The Division of Biomedical Engineering is involved in regional lung function studies, using the non-physiological radioactive gas ^{133}Xe , with a sixteen-probe detection system. As the Van de Graaff is physically situated relatively close to the Division of Biomedical Engineering, there was interest in producing a short-lived positron nuclide such as ^{11}C , ^{13}N or ^{15}O to label physiological gases for use in pulmonary studies. Carbon-11 labelled CO_2 was chosen for production and application to measurements of regional lung ventilation and perfusion. This work will be described in Chapter 4.

Fluorine-18 was chosen for production in response to the Department of Pharmacy which, in conjunction with the W.W. Cross Cancer Institute, was interested in a method of imaging tumors employing a short-lived positron emitter. To accomplish this, ^{18}F was incorporated

into the body in the form of ^{18}F -labelled 2'-deoxyuridine. These results will be discussed in Chapter 5.

The majority of medically useful positron-emitting nuclei are most easily produced by nuclear reactions. Once produced, the positron-emitting nuclide is proton unstable and has a probability of decaying via the conversion of a proton into a neutron, followed by the emission of a positron. A discussion of the theory of positron-emitting nuclide production and decay is presented in the following chapter.

CHAPTER 2

THEORY

2.1 Production of Radionuclides

The majority of positron-emitting nuclides are produced through nuclear reactions in which a change in the composition of a target nucleus is brought about through bombardment with a nuclear particle. When the target and bombarding nuclei approach each other within a distance of 10^{-13} cm, they experience a strong nuclear attraction, involving a redistribution of energy and momentum, which may give rise to different nuclei. The interaction mechanism involving the change from the initial to the final nuclear state is generally divided into two classes: one that proceeds directly to the final state and is known as a direct reaction, while the second proceeds through an intermediate state in which a compound nucleus is formed.

The probability of a particular nuclear reaction occurring may be expressed as a function of the nuclear cross section for that reaction, which is generally highly dependent upon the energy of the bombarding particle. The cross section plays the role of a target area surrounding each target particle and is generally expressed in units of barns (b), where $1\text{ b} = 10^{-24}\text{ cm}^2$.

Present theories of the cross section for reactions in which a compound nucleus is formed may be divided into two categories. At low bombarding energies (<10 MeV), the excited levels of the compound nucleus are discrete and widely separated. In this energy region the reaction cross sections are described by a resonance theory. At higher bombarding energies the excited levels of the compound nucleus are more closely spaced, broader and partially overlapping. This region is

described by a continuum theory. The production of positron-emitting nuclides at the University of Alberta is presently limited to the use of bombarding particle energies of less than 7 MeV, and therefore, we will only consider nuclear reactions described by the resonance theory.

Briefly, the resonance theory may be described as follows. (A more complete description is presented in reference 37.) The cross section for the formation of a compound nucleus by the capture of an incident particle may be expressed as the maximum cross section multiplied by the probability for the transmission through the nuclear barrier of a particle having an orbital angular momentum ℓ . If the localized effect of resonances is ignored, the overall transmission coefficient may be approximated by

$$T_a \approx \frac{4k}{K} P_a \quad (2.1)$$

where P_a is a Gamow type penetration factor³⁸ for the Coulomb and centrifugal barriers, and $4k/K$ is the probability that the incident particle can pass from outside the nucleus where its wave number is k to the region inside the nucleus where its wave number is K ($K \ll k$). The effect of the resonance levels is now superimposed upon the smoothly varying barrier transparency as shown in Figure 2.

If the bombarding energy, E , is in the neighborhood of a resonance of energy E_0 , the resonance may be represented by the function

$$f(E) = \frac{C}{(E-E_0)^2 + (\frac{\Gamma}{2})^2} \quad (2.2)$$

where Γ is the full width of the resonance measured at half maximum. The normalization constant C is evaluated such that the average value of $f(E)$ is unity when averaged over several resonances whose energy spacing

EFFECT OF RESONANCE LEVELS
ON THE
REACTION CROSS SECTION

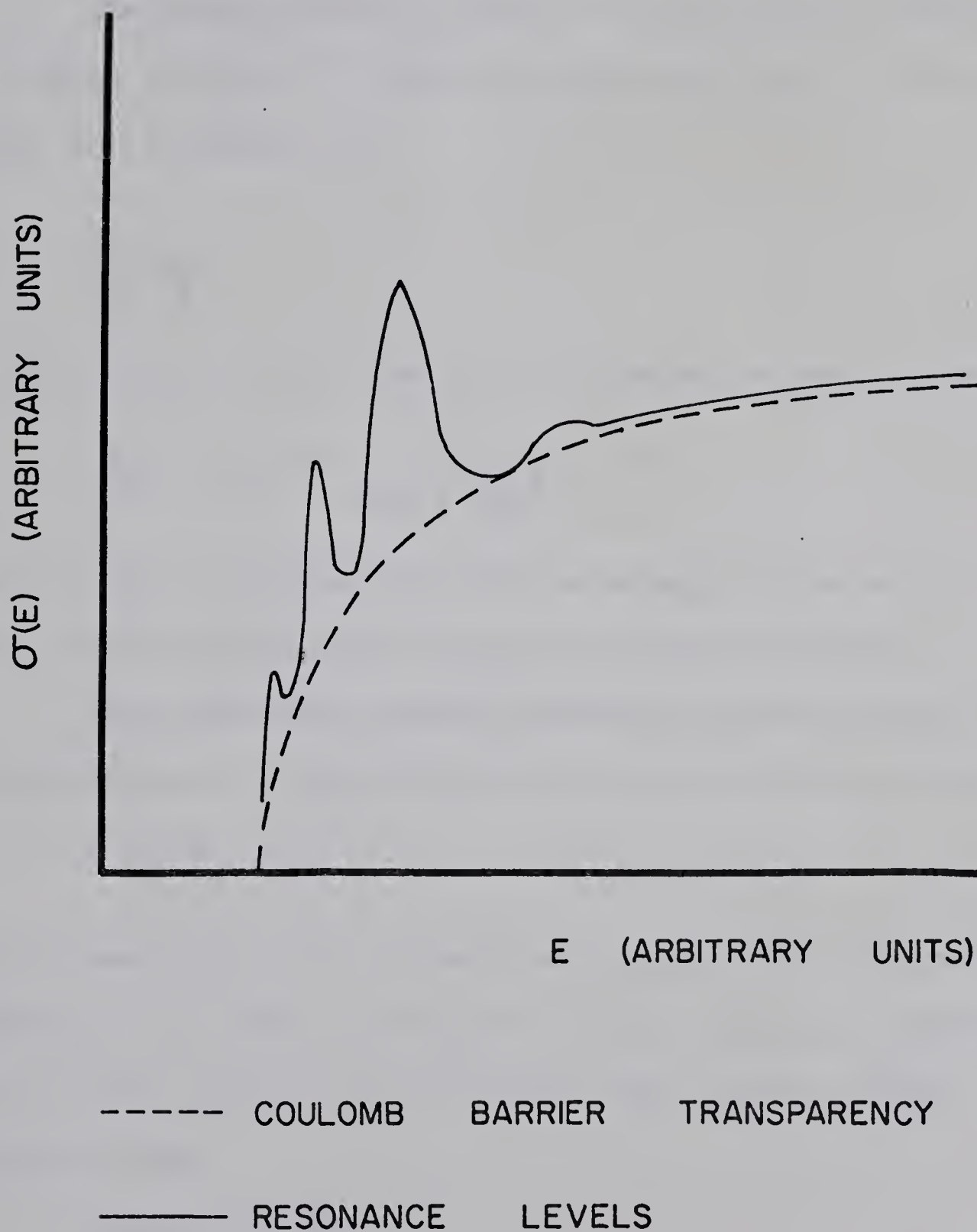


FIGURE 2

is D_ℓ , i.e.

$$\frac{1}{D_\ell} \int_{-\infty}^{+\infty} f(E) dE = 1 \quad (2.3)$$

which leads to $C = \frac{\Gamma D_\ell}{2\pi}$.

The average spacing of levels of orbital angular momentum ℓ , D_ℓ , is given in terms of T_a and the partial level width, Γ_a , for the capture of the particle a by

$$\frac{D_\ell}{2\pi} \approx \frac{\Gamma_a}{T_a}. \quad (2.4)$$

The cross section for the formation of a compound nucleus is then

$$\sigma_{CN}^\ell = \pi(2\ell+1)\lambda^2 \frac{\frac{\Gamma_a \Gamma}{2}}{(E-E_0)^2 + (\frac{\Gamma}{2})^2} \quad (2.5)$$

where λ is the rationalized de Broglie wavelength of the relative motion of the incident particle with respect to the target nucleus.

Once formed the compound nucleus may transform through any permitted channel i , each represented by a partial width Γ_i , where

$$\Gamma = \sum_i \Gamma_i, \quad (2.6)$$

and the summation is over all permitted channels. The fraction of transitions that follow any particular channel, say Γ_b , is simply Γ_b/Γ . Thus, the cross section for the reaction (a,b) through a single resonance becomes

$$\sigma(a,b) = \sigma_{CN}^\ell \frac{\Gamma_b}{\Gamma} \quad (2.7)$$

$$= \pi(2\ell+1)\lambda^2 \frac{\frac{\Gamma_a \Gamma_b}{2}}{(E-E_0)^2 + (\frac{\Gamma}{2})^2} \quad (2.8)$$

If a or b are charged particles the partial widths Γ_a and Γ_b will contain Coulomb penetration factors.

The presence of resonances acts to increase to the cross section. Therefore, it is desirable to have the bombarding energy centered on a resonance of the reaction in order to increase the quantity of the radionuclide produced. The resonances of the $^{11}\text{B}(\text{p},\text{n})^{11}\text{C}$ and $^{20}\text{Ne}(\text{d},\alpha)^{18}\text{F}$ reactions appear in Figures 9 and 15 respectively.

Several quantities are conserved in strong nuclear reactions, among them being charge, parity, and the total energy and total momentum of the system. The conservation of energy may be expressed through the Q-equation. Consider that the nuclear reaction is initiated by an incident particle of mass M_I and kinetic energy T_I reacting with a target nucleus of mass M_T and kinetic energy T_T . After the reaction, either through a compound nucleus or intermediate system, an emitted particle of mass M_E and kinetic energy T_E leaves a residual nucleus of mass M_R and kinetic energy T_R . The general dynamics of this two-body nuclear reaction are shown in Figure 3. The Q-equation can be taken as an analytic relationship between the nuclear disintegration energy, Q , and the kinetic energy of the initial and final particles as measured in laboratory coordinates. Since the Q value is proportional to the change in rest mass, it has the same value in the laboratory coordinates as in the center of mass coordinates.³⁹ Taking the target nucleus to be at rest, conservation of mass-energy for an isolated system gives

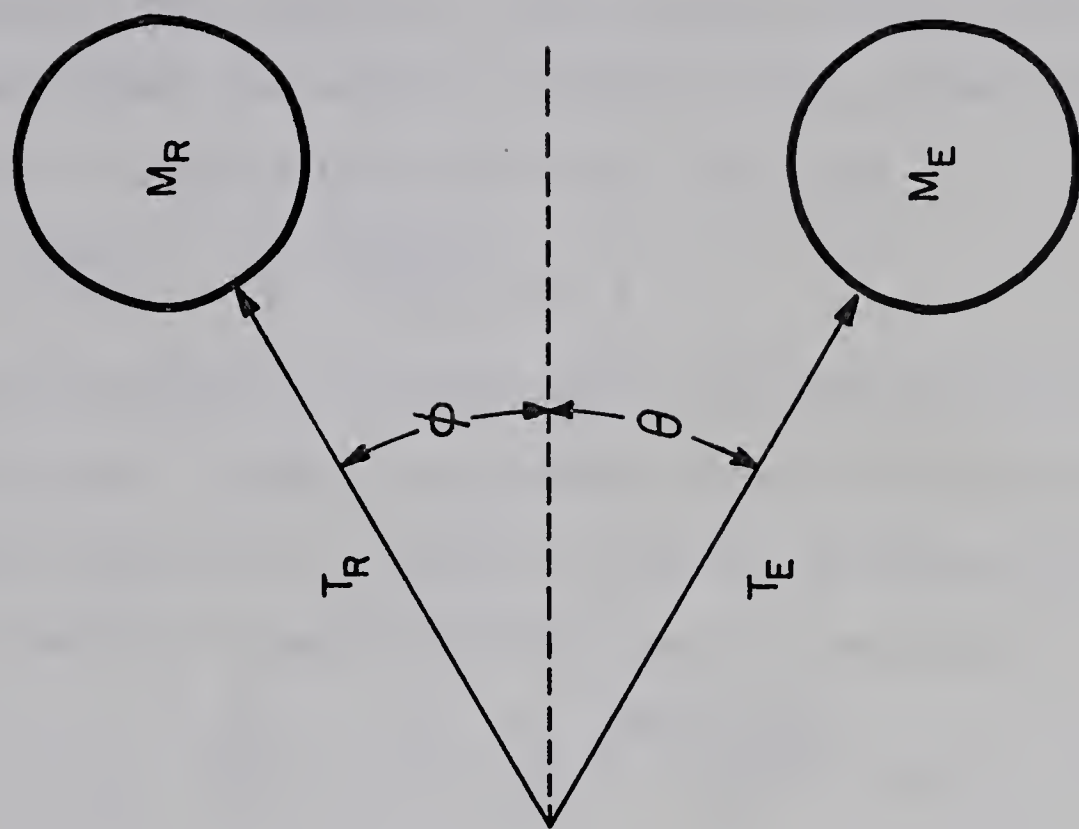
$$T_I + Q = T_E + T_R. \quad (2.9)$$

From conservation of linear momentum in the direction of the incident particle we have

TWO BODY REACTION KINEMATICS

BEFORE COLLISION

AFTER COLLISION



$$T_T = 0$$



FIGURE 3

$$\sqrt{2M_I T_I} = \sqrt{2M_E T_E} \cos \theta + \sqrt{2M_R T_R} \cos \phi. \quad (2.10)$$

As the initial linear momentum in the direction normal to the plane containing the incident and emitted particles is zero, θ and ϕ are coplanar. Conservation of momentum in the θ - ϕ plane then gives

$$\sqrt{2M_E T_E} \sin \theta - \sqrt{2M_R T_R} \sin \phi = 0. \quad (2.11)$$

A simultaneous solution of equations 2.9, 2.10, and 2.11 can eliminate any two parameters. Usually, the kinetic energy and the direction ϕ of the residual nucleus are eliminated to give the conventional form of the Q-equation, which is independent of the reaction mechanism:

$$Q = T_E \left(1 + \frac{M_E}{M_R}\right) - T_I \left(1 - \frac{M_I}{M_R}\right) - \frac{\sqrt{2 M_I T_I M_E T_E}}{M_R} \cos \theta. \quad (2.12)$$

The kinetic energy of the incident and emitted particles and the angle θ are measured in the laboratory coordinates.

For values of $Q > 0$, the nuclear reaction results in the liberation of rest energy due to a reduction in the rest mass of the products and is called an exoergic reaction. Such a reaction can proceed when the incident particle has sufficient energy to overcome the Coulomb barrier of the target nucleus. The case of $Q=0$ corresponds to the elastic scattering of the incident particle in which the rest mass and kinetic energy are conserved. For $Q < 0$, the reaction results in a decrease of kinetic energy due to the increase in the rest mass of the products and is called an endoergic reaction. For an endoergic reaction to take place, the kinetic energy of the incident particle must be greater than some predefined value. The threshold energy is the smallest value of the bombarding energy for which the reaction can take place. As a function of the angle θ , the threshold energy is given by

$$(T_I)_{\text{Thr}} = -Q \left[\frac{\frac{M_E + M_R}{M_E + M_R - M_I - \frac{M_I M_E}{M_R} \sin^2 \theta}}{\frac{M_E + M_R - M_I}{M_E + M_R - M_I} \sin^2 \theta} \right]. \quad (2.13)$$

The threshold energy will have its minimum value at $\theta=0^\circ$ where Eq. 2.13 becomes

$$(T_I)_{\text{Thr}} \Big|_{\theta=0} = -Q \left[\frac{\frac{M_E + M_R}{M_E + M_R - M_I}}{\frac{M_E + M_R - M_I}{M_E + M_R - M_I}} \right]. \quad (2.14)$$

Utilizing the relationship between Q and the rest masses

$$M_I + M_T = M_E + M_R + \frac{Q}{c^2}, \quad (2.15)$$

and since $M_T \gg \frac{Q}{c^2}$, Eq. 2.14 becomes

$$(T_I)_{\text{Thr}} \Big|_{\theta=0} = -Q \left[\frac{\frac{M_I + M_T}{M_T}}{\frac{M_E + M_R - M_I}{M_E + M_R - M_I}} \right]. \quad (2.16)$$

Consider as an example the endoergic reaction $^{11}\text{B}(p,n)^{11}\text{C}$, which has a Q value of -2.763 MeV. The threshold energy follows from Eq. 2.16:

$$(T_I)_{\text{Thr}} \Big|_{\theta=0} = 2.763 \frac{(1 + 11)}{11} \text{ MeV} = 3.02 \text{ MeV}. \quad (2.17)$$

If the incident particle has a charge it must also have enough energy to overcome the Coulomb barrier of the nucleus. The Coulomb barrier results from the positive charge of both the incident and target nuclei. If the Coulomb barrier is represented by

$$U(r) = 0 \quad r < R \quad (2.18)$$

$$U(r) = \frac{Zze^2}{r} \quad r > R \quad (2.19)$$

where Z = charge of the target nucleus,

z = charge of the incident particle,

R = effective radius of the target nucleus = $1.3 \times 10^{-13} A^{1/3} \text{ cm}$,

A = number of nucleons in the target nucleus,

r = distance from the centre of the target nucleus,
and $e = 1.6 \times 10^{-19}$ Coulombs,

the Coulomb barrier B is

$$B = \frac{Zze^2}{R} . \quad (2.20)$$

For the $^{11}\text{B}(p,n)^{11}\text{C}$ reaction the Coulomb barrier is 2.16 MeV.

The incident particle can have a nonzero probability of penetrating the Coulomb barrier even if its energy is less than that needed to overcome the barrier. This effect, called "barrier transmission", is most probable for those particles which undergo central collisions. In this case no energy goes into rotational motion and all of the initial energy of the particle is available to attack the Coulomb barrier. The collisions which involve no change in angular momentum are called $\ell=0$ or s-wave collisions. For these, the transmission probability T_0 of an incident nucleon through the potential barrier is

$$T_0 \approx e^{-\gamma} \quad (2.21)$$

where

$$\gamma = \frac{8\pi Zze^2}{hv} \left[\cos^{-1} \sqrt{\frac{T}{B}} - \sqrt{\left(\frac{T}{B}\right)\left(1-\frac{T}{B}\right)} \right] \quad (2.22)$$

and

T = kinetic energy of the incident particle in the center of mass coordinates,

v = velocity of the incident particle in laboratory coordinates,

and h = Planck's constant.

As an example, consider the $^{11}\text{B}(p,n)^{11}\text{C}$ reaction. The energy which the incident proton must have in order that 50 per cent of the protons are

transmitted through the Coulomb barrier is approximately 1 MeV.

The effective Q value for a nuclear reaction is composed of two parts: the threshold Q value relating the energy difference between the initial and final state, and the Coulomb Q value, Q_C , indicating the energy necessary to overcome the Coulomb barrier:

$$Q_{\text{Eff}} = Q_{\text{Thr}} + Q_C . \quad (2.23)$$

In the above example the effective Q value, assuming 50 per cent barrier transmission, is 4 MeV.

The following table lists some positron-emitting nuclides with half-lives between two minutes and twenty-four hours, which could be produced with the 7 MV Van de Graaff at the University of Alberta in quantities greater than 50 μCi .

TABLE 1

A list of some positron-emitting nuclides producible with a
7 MV Van de Graaff.

<u>Nuclide</u>	<u>Half-life</u>	<u>Nuclide</u>	<u>Half-life</u>
^{11}C	20.5 min.	^{76}Br	17.2 hr.
^{13}N	9.96 min.	^{97}Rh	35 min.
^{15}O	2.2 min.	^{98}Rh	8.7 min.
^{18}F	110 min.	^{102}Ag	16 min.
^{30}P	2.5 min.	^{107}In	33 min.
^{38}K	7.7 min.	^{108}In	40 min.
^{43}Sc	3.9 min.	^{115}Sb	60 min.
^{47}V	32 min.	^{121}I	120 min.
^{49}Cr	42 min.	^{131}La	58 min.
^{51}Mn	45 min.	^{132}La	4.5 hr.
^{62}Cu	9.8 min.	^{136}Pr	70 min.
^{64}Ga	2.6 min.		
^{68}Ga	68 min.		
^{70}As	52 min.		

2.2 Yield of Radionuclides

The yield of radioactive nuclei produced through a nuclear reaction is the net rate at which new nuclei are produced under specified bombardment and target conditions. Consider the production of a nuclide B from A via the reaction $A(x,y)B$. Let the number of target atoms of A which are accessible to the beam of bombarding particles be N'_A and the probability of transforming an atom of A into an atom of B be P_A . Then the rate of production of B is $P_A N'_A$. The probability of the transformation P_A is equal to σN_x , where σ is the cross section for the nuclear reaction and N_x the number of bombarding particles per unit area per unit time interacting with the atoms A. The rate of production of B is then $\sigma N_x N'_A$.

If B is radioactive, there is a probability, P_B , of B decaying to an atom C. Let the number of atoms of B at time t during the production be N'_B . Then,

$$\frac{dN'_B}{dt} = N'_A P_A - N'_B P_B. \quad (2.24)$$

If the only source of the atoms of A is from the initial supply,

$$N'_A = N_A e^{-P_A t} \quad (2.25)$$

where $N_A = N'_A$ at $t=0$. Equation 2.24 then becomes

$$\frac{dN'_B}{dt} = P_A N_A e^{-P_A t} - N'_B P_B. \quad (2.26)$$

The general solution to

$$N'_B = N_A (ae^{-P_A t} + be^{-P_B t}) \quad (2.27)$$

where a and b are constants. To evaluate a and b we substitute the expression for N'_B into Eq. 2.26, which yields

$$N_A e^{-P_A t} (-aP_A - P_A + aP_B) = 0. \quad (2.28)$$

For Eq. 2.28 to remain valid for all times t , it is necessary that

$$-aP_A - P_A + aP_B = 0 \quad (2.29)$$

from which it follows that

$$a = \frac{P_A}{P_B - P_A}. \quad (2.30)$$

For the special case where $N'_B = 0$ at $t=0$, we have from Eq. 2.27

$$a+b = 0 \text{ or } a = -b. \quad (2.31)$$

Therefore, the number of atoms of B at time t becomes

$$N'_B = N_A \frac{P_A}{P_B - P_A} (e^{-P_A t} - e^{-P_B t}) \quad (2.32)$$

for the condition $N'_B = 0$ at $t=0$. The activity of B is

$$N_B P_B = N_A P_A \frac{P_B}{P_B - P_A} (e^{-P_A t} - e^{-P_B t}). \quad (2.33)$$

The yield, Y , is the rate at which new activity is formed. In the special case of a first daughter product, the yield is constant and equal to the initial slope of the growth curve for the activity formed:

$$Y = \left(\frac{d(N'_B P_B)}{dt} \right)_{t=0}. \quad (2.34)$$

Substituting Eq. 2.32 into Eq. 2.34 we obtain

$$Y = N_A P_A \frac{P_B}{P_B - P_A} (-P_A e^{-P_A t} + P_B e^{-P_B t})_{t=0} \quad (2.35)$$

$$= N_A P_A P_B. \quad (2.36)$$

Usually, only a negligible fraction of the target atoms A, is transformed so that the number of residual target atoms $N'_A = N_A e^{-P_A t}$, may be approximated as N_A . The rate for the production of B now becomes

$$N_A' P_A = \frac{Y}{P_B} = Y\tau_B \quad (2.37)$$

where τ_B is the mean life of B.

In the case of the production of short-lived positron-emitting nuclides, the daughter nucleus B is much shorter lived than the parent nucleus A. The resulting activity of B takes on a particularly simple form when $P_A \ll P_B$. From Eq. 2.32

$$N_B' P_B = N_A P_A (1 - e^{-P_B t}) \quad (2.38)$$

or

$$N_B' P_B = Y\tau_B (1 - e^{-P_B t}) \quad (2.39)$$

which is the net activity of B which can be accumulated in a time t. From Eq. 2.39, the maximum activity that can be produced is $Y\tau_B$. The exponential growth of the activity of B (Eq. 2.39) is plotted in Figure 4 as a function of the half period, T, and $Y\tau_B$. The rates of production and decay become approximately equal after a bombarding time of about six half-periods.

2.3 Positron Decay

Positron decay⁴⁰⁻⁴² is the spontaneous transformation of an unstable nucleus accompanied by the emission of a positron. The decay of an unstable nucleus by positron emission is one of the three forms of beta decay, the other two being decay through the emission of an electron or through the capture of an orbital electron by the unstable nucleus. The nuclear transformation resulting from positron decay is from an unstable nucleus of charge Z and mass M(Z) to a nucleus of charge Z-1 and mass M(Z-1). A proton in the unstable nucleus is transformed into a neutron accompanied by the release of a positron and a

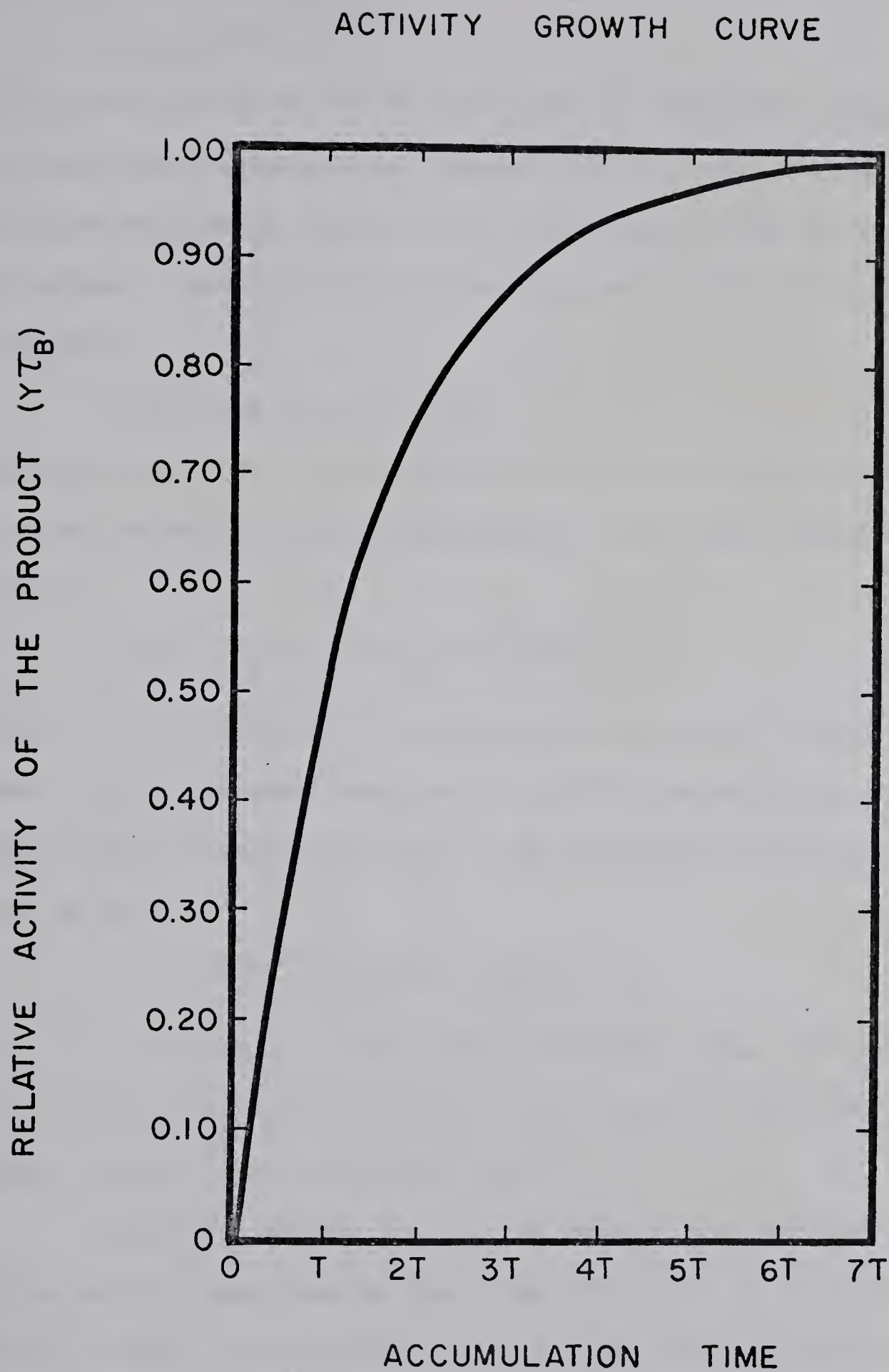
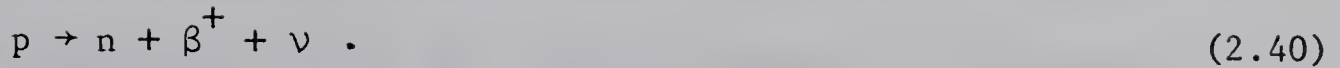


FIGURE 4

neutrino:



As the mass of a proton is less than that of a neutron, positron decay of a free proton cannot occur. However, for a proton within the nucleus the transformation is possible since the necessary energy is supplied by the nucleus. The relationship between nuclear masses for positron decay is given by

$$M(Z) = M(Z-1) + m_o + E/c^2 \quad (2.41)$$

where m_o is the mass of the positron and E is the kinetic energy of the positron, neutrino and recoiling nucleus. For atomic masses Eq. 2.41 becomes

$$M_A(Z) = M_A(Z-1) + 2m_o + E/c^2 - I/c^2 \quad (2.42)$$

where I is the difference in electron binding energy between the two atoms. Since I is small compared to the other terms in Eq. 2.42 it is usually omitted from calculations. The energy released in positron decay is then

$$E = (M_A(Z) - M_A(Z-1) - 2m_o)c^2 . \quad (2.43)$$

Note that in contrast to other types of nuclear decay, the positron decay energy is not directly equal to the change in the neutral atomic masses, but must be decreased by $2m_o c^2$.

After the nucleus decays, the emitted positron may combine with an electron and form an atom of positronium. In quantum mechanical terms, the atom of positronium may be thought of as analogous to the hydrogen atom with the positron replacing the proton. All the various quantum numbers which describe the hydrogen atom can be ascribed to positronium. It is thought that electrons in states of high orbital

angular momentum undergo successive radiative transitions until they reach the S(ground)-state of zero angular momentum. The S-state of the positronium atom can exist in the singlet state with the spins of the positron and electron antiparallel or in the triplet state with their spins parallel. Decaying by two quantum annihilation, the mean lifetime of positronium in the singlet state is approximately 10^{-10} seconds. Annihilation from the triplet state requires three quantum annihilation which is a forbidden transition with a mean lifetime of approximately 10^{-7} seconds.

Most positron annihilation radiation results from the singlet state of positronium. When the positron and electron combine and annihilate, two gamma rays are emitted with an energy totalling the combined mass of the positron and electron, $2m_0c^2$. If the momentum of the center of mass of the positronium atom is zero in the laboratory system, the two gamma rays emitted will each have an energy of $m_0c^2 = 511 \text{ keV}$ and travel at 180 degrees from each other. However, it has been found experimentally⁴³ that due to thermal agitation the average momentum of the center of mass is approximately $0.009m_0c^2$. This leads to an angular distribution of ± 0.5 degrees about 180 degrees for the two emitted gamma rays. Another mode of decay that has a finite probability of occurring is the annihilation of "swift" positrons which occur in about two per cent of the interactions. In this case the initial momentum of the center of mass is quite large and approximately one-half of the resulting photons will have an energy significantly greater than 511 keV.

Some insight into positron decay may be obtained from the concept of allowed and forbidden nuclear transitions in beta decay.

Nuclear transformations are most probable if the change in angular momentum between the initial and final states is the minimum possible value and if there is no change in parity. In 1933, Sargent⁴⁴ correlated the maximum energy of the beta spectrum with the half-life of various nuclides. He noticed that the nuclides fell into two groups, one group having half-lives approximately 100 times the others. In 1934, Gamow⁴⁵ proposed that the nuclear angular momentum was responsible for the two groups. He suggested that the shorter lived group followed "allowed" transitions with a selection rule of no change in angular momentum and no change in parity. The longer lived group followed "forbidden" transitions with a change in nuclear angular momentum of ± 1 and a change in parity between the initial and final state. However, since this initial work, newly discovered beta emitters were found which did not fit into this scheme. The forbidden transitions were subsequently divided into first forbidden, second forbidden, third forbidden, and so on, with each of these classes further subdivided into favored and unfavored transitions.

To compare the half-life values of beta emitters in the different transition classes, a comparative half-period or f_t classification was introduced by Konopinski⁴⁶. His theory allowed comparison of the observed half-periods t after allowance had been made through a function "f" accounting for differences in nuclear charge and the energy of the beta transition. From the theory of allowed transitions it was found that,

$$f_t = \frac{\text{universal constant}}{|P|^2} \quad (2.44)$$

where $|P|^2$ is the nuclear matrix element for the transition. A special

class of allowed and favored or "superallowed" transitions⁴⁷ were found to exist for mirror nuclei with ft values between 1×10^3 and 5×10^3 seconds. The allowed and unfavored transitions have ft values between 5×10^3 and 5×10^5 seconds. It is usual to speak of log ft values rather than ft values due to the large size of the numbers. The log ft values for superallowed, allowed, and first forbidden transitions are respectively 3, 3 to 5, and 6 to 8. The positron transitions of $^{11}\text{C} \rightarrow ^{11}\text{B}$ and $^{18}\text{F} \rightarrow ^{18}\text{O}$ fall in the class of superallowed and allowed transitions respectively.

CHAPTER 3
FACILITY FOR ISOTOPE PRODUCTION

3.1 Introduction

The production of short-lived positron-emitting nuclides requires a source of nuclear particles of sufficiently high energy with which to bombard a target nucleus so that it will readily undergo a nuclear reaction, transforming it into a positron emitter. Two sources of such particles are the particle accelerator and the nuclear reactor, with the majority of the short-lived positron emitters being produced with particle accelerators. The two main types of particle accelerators used for radionuclide production are the electrostatic generator and the cyclotron.

The Van de Graaff accelerator at the University of Alberta is an electrostatic generator. It is capable of accelerating hydrogen, deuterium, helium-3 or helium-4 ions through a potential difference of approximately 7 MV. Figure 5 shows the principle of operation⁴⁸ of a Van de Graaff. A moving insulated belt charged positively by corona discharge at the base of the machine transports this charge to the top of the machine at which point another corona discharge removes the positive charge from the belt, transferring it to the terminal sphere. In this manner, the terminal end of the Van de Graaff can be charged up to a maximum of 7 MV. The highly charged terminal sphere is connected to the accelerator tube into which positively charged ions are injected at the top. These ions are then accelerated down the tube by the electrostatic field. The Van de Graaf accelerator is enclosed in a pressurized vessel containing an insulating mixture of N₂ and SF₆ gas which suppresses electrical discharge and prevents destructive fires.

SCHEMATIC DIAGRAM OF VAN DE GRAAFF

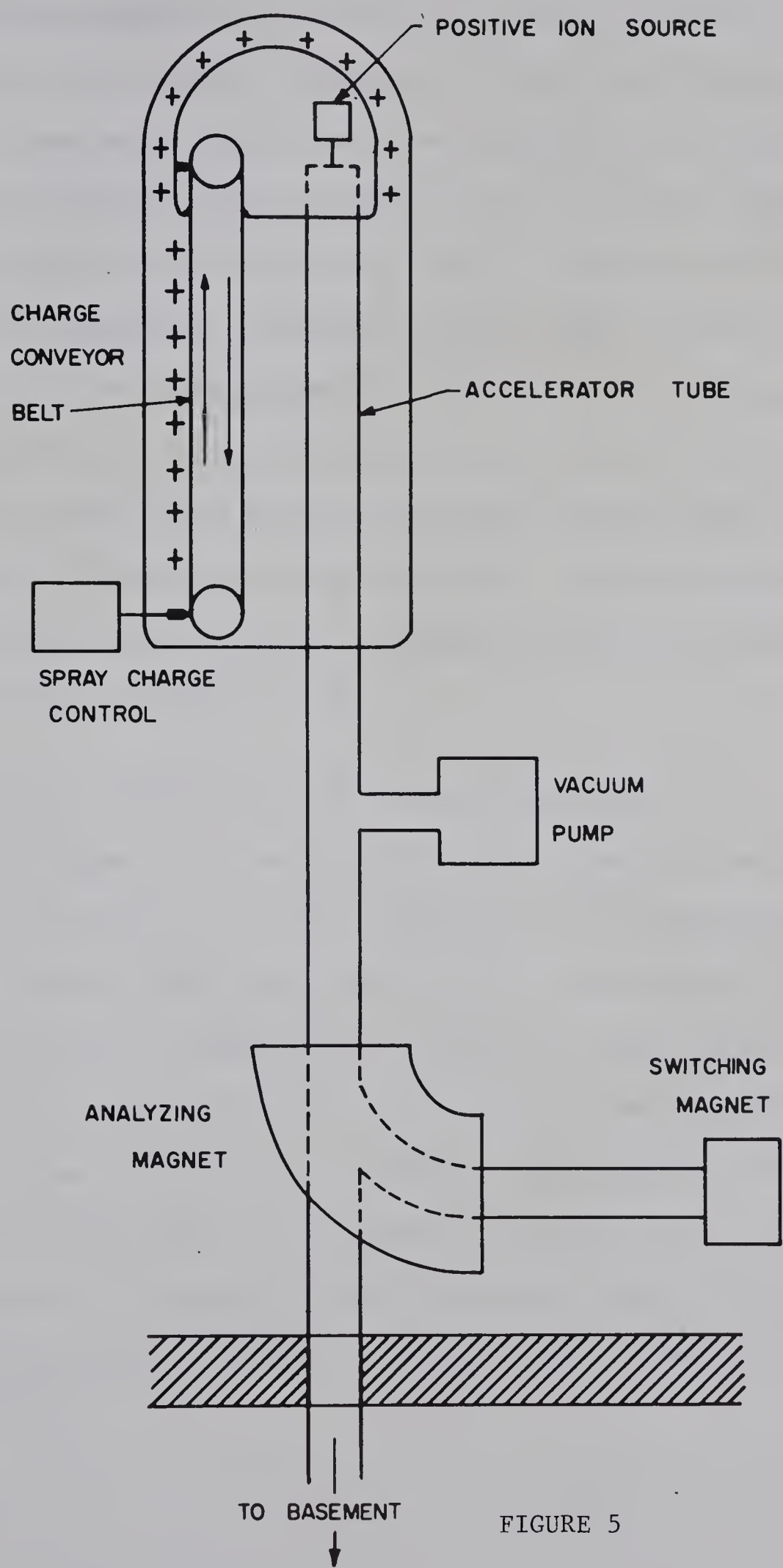


FIGURE 5

For the efficient production of positron-emitting nuclides, the accelerated beam should possess sufficient energy to allow the nuclear reaction to proceed and a high beam current well focused on the target. It is important to monitor various parameters of the experiment is to ensure the production of the radionuclide of interest. Important aspects during the production are: the status of the Van de Graaff, the vacuum in the accelerator and beam transport tubes, characteristics of the accelerated beam, and the amount of beam striking the target. During the production it is also necessary to protect the Van de Graaff should a failure occur either in the irradiation cell or within the accelerator and associated beam line components. Another important aspect to consider is that adequate shielding be provided to maintain the radiation within acceptable limits.

3.2 Construction of the Facility for Isotope Production

Initial experiments for the production of positron-emitting nuclides were carried out in the main target room. The reactions used to produce the radionuclides were found to yield a high neutron flux which proved difficult to shield with the existing target room facility. In order to keep the radiation within safe levels, it was necessary to keep the beam current relatively low ($\approx 300\text{nA}$). This beam restriction adversely affected the quantity of radioactivity which could be produced, and therefore a new facility was constructed which provided adequate shielding while allowing an increase in beam current to approximately 20 μA .

The new facility was constructed directly beneath the Van de Graaff in the basement of the Nuclear Research Center. The placement of this facility offered two immediate advantages. The first was an overall increase in beam current since the new beam line had no momentum analysis. The second was ease in providing the necessary shielding for the experiment. The floor and three of the walls in the new target room were surrounded by earth, and the forward motion of the beam was directed at the floor of the room. Therefore, it only remained to shield the remaining wall and prevent the neutrons from being scattered upwards.

To provide adequate shielding from the radiation resulting from the production of positron-emitting nuclides it was first necessary to determine the type of radiation. The nuclear reactions used in the production of ^{11}C and ^{18}F both produce neutrons as a direct consequence of the beam interacting with the target. This type of radiation, directly associated with the operation of the Van de Graaff, is referred to as a prompt radiation field. An understanding of the prompt radiation field requires knowledge of the primary interaction in the target and the subsequent interactions of the reaction products with the accelerator structure and surrounding experimental materials and shielding. A second radiation field may be described as a residual field, since it remains after the accelerator is turned off. In this case, the main source of the radiation field is the gamma radiation involved in the decay of the positron-emitting nuclides. Residual field shielding will be discussed in Chapter 4.

The 6.30 MeV proton beam used in the production of ^{11}C through the $^{11}\text{B}(\text{p},\text{n})^{11}\text{C}$ reaction produces⁴⁹ a neutron flux of approximately

1×10^6 neutrons/(\(\mu\text{A}\cdot\text{sec}\cdot\text{ster}\)), which is the main source of the prompt radiation field. The beam of protons incident on the B_2O_3 target provides a beam of neutrons predominantly forward scattered with energies of approximately 3-4 MeV.⁵⁰ The 6.5 MeV deuteron beam used in the production of ^{18}F through the $^{20}\text{Ne}(\text{d},\alpha)^{18}\text{F}$ reaction produces a prompt radiation field of neutrons via the deuteron stripping process. In this process, a target nucleus has a certain probability of capturing the proton of the bombarding deuteron, permitting the neutron to continue in the forward direction with approximately one-half of the original deuteron energy. Another source of prompt radiation in the ^{18}F reaction is due to the ionizing action of the alpha particle. However, this does not contribute significantly to the prompt field. The prompt radiation field in both the $^{11}\text{B}(\text{p},\text{n})^{11}\text{C}$ and $^{20}\text{Ne}(\text{d},\alpha)^{18}\text{F}$ reactions is dominated by fast neutrons, where a fast neutron is generally defined as having an energy greater than 1 MeV. Neutron radiation is attenuated by the inverse square of the distance between the source and the observer and by absorbing and scattering the neutrons in a solid barrier of the appropriate material.

To provide adequate neutron shielding, it is important to understand how neutrons interact with matter.⁵¹⁻⁵⁴ Since the neutron carries no electrical charge it will not produce ionizing radiation directly, but instead will interact with the nucleus in interactions which are strongly dependent upon the neutron energy. Inelastic scattering of neutrons by nuclei occurs when the neutron energy is in the region of 1 to 10 MeV. In this case, the nucleus absorbs the neutron and recoils. A slower neutron is then emitted along with gamma radiation. The probability for the inelastic scattering of

neutrons increases as the atomic number of the target nucleus increases.⁵⁵ For neutrons in the energy region of 1 MeV to 0.01 MeV, the main mode of interaction is by elastic scattering, particularly with very light nuclei. In elastic scattering the neutron can lose some or all of its energy to a recoiling nucleus. At neutron energies less than 0.01 MeV, the neutron may undergo radiative capture, in which it is absorbed by the nucleus, with the nucleus recoiling and emitting a proton or alpha particle accompanied by gamma radiation.

The important steps in the shielding of fast neutrons are first to slow the neutrons down through inelastic scattering with heavy nuclei and then to remove them from the radiation field through elastic scattering and radiative capture. The presence of hydrogen in the shielding medium has a marked effect upon neutron attenuation, since the interaction cross section of hydrogen for neutrons has a high absolute value which increases with decreasing neutron energy.⁵⁶ As a result of an interaction with hydrogen, a neutron experiences an average loss of one-half of its initial energy, as it has essentially the same mass as the hydrogen atom; this loss of energy increases with increasing angle of scatter of the neutron. The differential neutron scattering cross sections of hydrogen are isotropic in the center of mass system in contrast to heavy nuclei where there is a higher probability of scattering in the forward direction. Therefore, it is advantageous to use hydrogen in the shielding medium because any interaction of neutrons with these nuclei causes either a decrease in the initial neutron energy or scattering at large angles from the initial direction, thus greatly reducing the probability of neutrons passing through the shielding.

In the design of the shielding enclosure for the radionuclide production facility, concrete was chosen as the major component as it contains enough hydrogen to be an effective neutron shield. To limit the radiation to a small area near the actual radionuclide production site, a small enclosure was built around the end of the beam tube (see Figure 6). The walls of the enclosure were built from concrete blocks to a total thickness of 0.59 m and an inside height of 1.97 m (Figure 7). To prevent skyshine caused by the backward scattering of neutrons, a roof was constructed on the enclosure consisting of 2.5 cm of steel plate to moderate the neutrons and 0.41 m of concrete blocks to reduce the neutron flux. Calculations⁵⁷ have shown that the design of such an enclosure should attenuate the neutron flux by a factor of approximately 500. To test the effectiveness of the shielding under normal operating conditions, a "tissue equivalent" dose-rate for neutrons was measured inside the enclosure for comparison with that measured outside. The neutron dose inside the enclosure was 3.5 ± 0.2 rem/hr while the dose measured immediately outside the wall was 10 ± 2 mrem/hr. Thus, the effectiveness of the shielding in the horizontal direction is such to reduce the tissue equivalent dose by a factor of approximately 350.

3.3 Monitoring of Beam Conditions

In order to control the amount of beam striking the target it is necessary to monitor the various effects the accelerator has on the beam characteristics. Some of the beam characteristics that should be monitored are: the beam current, reflecting the amount of bombarding ions present, the position of the beam relative to the target and the spatial distribution of the beam normal to its flight path.



SIDE VIEW OF SHIELDING ENCLOSURE

TOP VIEW OF SHIELDING ENCLOSURE

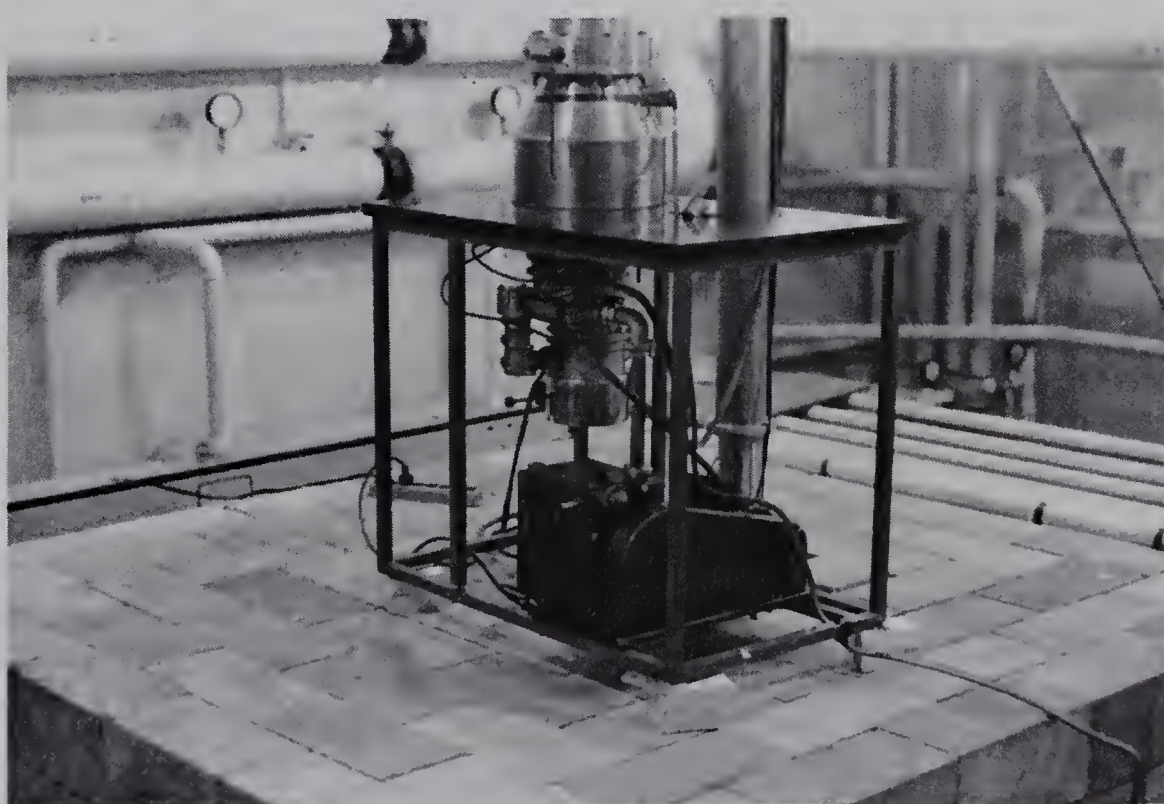


FIGURE 6

FLOOR PLAN OF SHEILDING ENCLOSURE

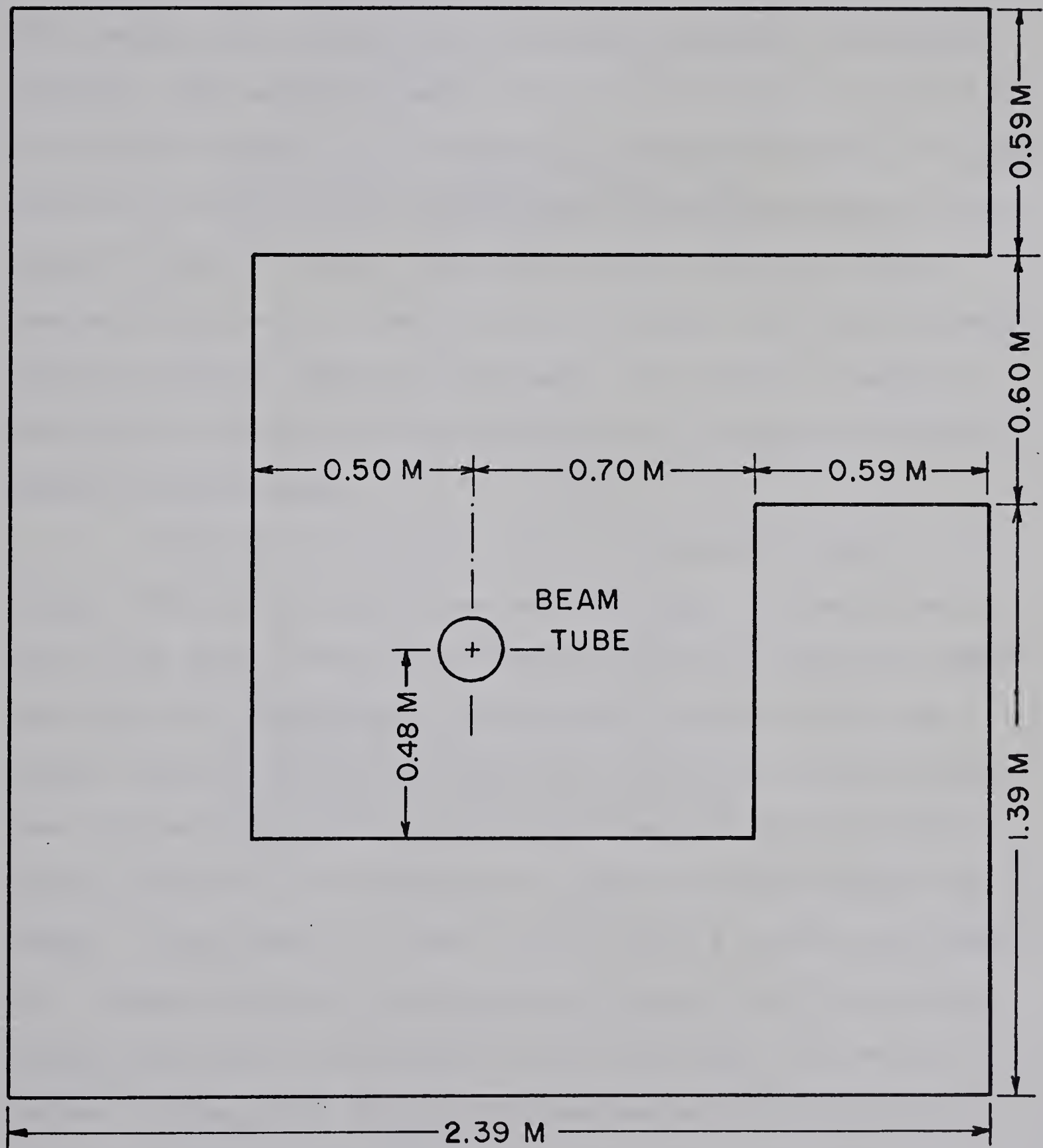
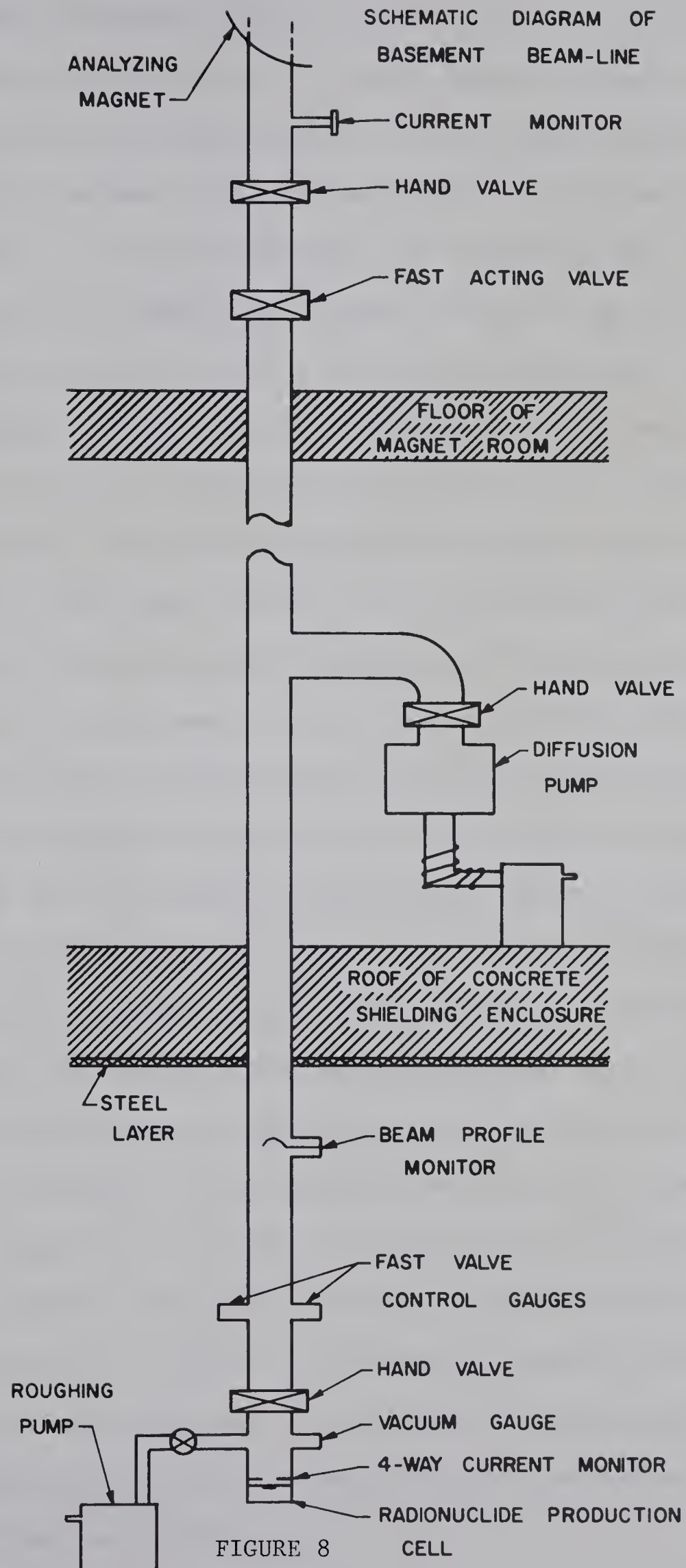


FIGURE 7

In the new facility there are two positions for monitoring the beam current along the beam line. One is just below the analyzing magnet while the other is on the target of the radionuclide production cell (see Figure 8). The current monitor below the analyzing magnet consists of a Faraday cup to collect the beam current during the initial beam focusing. This monitor is water cooled, thus allowing it to be left in place until a stable beam is obtained after which the monitor is removed from the beam path and the beam allowed to travel down toward the radionuclide producing facility. The second monitor provides a direct reading of the amount of beam striking the target; this value is used as an aid in focusing the beam on the target. The current on target is also used in calculations predicting the quantity of positron-emitting nuclides being produced.

Two monitors are used to locate the beam with respect to the target. One is a four-way current monitor located 10 cm above the target and the other a beam profile monitor located 30 cm above the target (see Figure 8). The four-way current monitor consists of four pie-shaped pieces of 0.5 mm thick tantalum. Each section is electrically insulated and the monitor constructed with the four sections equally spaced around a 0.5 cm diameter hole to allow the beam through to the target. If the beam is off axis, it will strike a section of the monitor. Through refocusing, the beam can be "steered" off that section, through the center of the monitor and onto the target. The second monitor, a beam profile monitor, developed and marketed by National Electrostatics Corporation, is used to measure the intensity distribution and position of a beam of charged particles. A single wire



formed into a 45-degree helix is rotated about its longitudinal axis in the vacuum of the beam tube. It sweeps across the beam in two orthogonal directions approximately nineteen times a second. The secondary electron current released from the wire as it intercepts the beam is a measure of the beam intensity. The horizontal axis of the monitor can be adjusted to display an accurate profile of the beam thus facilitating accurate centering of the beam with respect to the target and providing a cross sectional visualization of the beam.

A separate control unit was constructed to aid in monitoring the experiment. This module displays the open or closed status of each valve in the production facility. It also coordinates the current measurement of the two current monitors and the four-way current monitor and permits the measurement of the temperature within the target cell.

A separate vacuum system was installed for the new facility to maintain the high vacuum necessary for efficient Van de Graaff operation. The system was constructed to independently maintain a vacuum of approximately 1×10^{-6} Torr in the section below the fast-acting valve. Two different pumping stations were incorporated, one, a mechanical pump located near the bottom of the beam tube and the other, a six-inch mercury diffusion pump and cold trap located on the roof of the shielding enclosure. The mechanical pump was used to lower the pressure to approximately 5×10^{-3} Torr, at which point the diffusion pump and cold trap further lowered the pressure and maintained the vacuum at approximately 1×10^{-6} Torr. A thermocouple gauge was used to monitor the vacuum at the pressures at which the mechanical pump operated. A Philips ion gauge was used for remote high vacuum monitoring while the experiment was in progress.

3.4 Protection of the Van de Graaff

To understand the need for a system to protect the Van de Graaff against a failure in the experiment, a brief explanation of the radionuclide production cell is necessary. The beam of incident particles from the Van de Graaff enters the production cell through a 5×10^{-3} mm thick molybenum foil. This thin foil separates the vacuum in the beam tube from atmospheric pressure within the radionuclide production cell. As the incident particles pass through the foil, some of their energy is lost and appears in the form of heat. Should this heat be allowed to build up, the beam could eventually burn a hole in the foil causing it to rupture. To reduce the chance of this happening, the foil is water cooled. However, if a failure should occur in the experiment causing the foil to rupture, the gas at atmospheric pressure in the production cell would rush into the vacuum of the beam tube forming a destructive shock wave that could travel with a velocity as high as 965 m/sec. To prevent this shock wave from damaging the Van de Graaff, a fast-acting valve was installed in the beam line that will close should an increase in the pressure of the vacuum section occur. A 25 msec fast-acting valve and associated electronics were chosen to protect the Van de Graaff. The valve was located as far as possible from the entrance foil of the gas cell and yet within the beam line used for radionuclide production. This valve was installed just below the analyzing magnet, approximately ten meters from the entrance foil and vacuum sensors. The vacuum sensors consist of two vacuum gauges, each one capable of releasing the valve. The gauge supplied by the manufacturer will close the valve if the pressure rises above 1×10^{-2} Torr. To increase the protection, an

additional gauge was installed to close the valve in the event that the pressure rises above 1×10^{-4} Torr. Should a rupture in the foil occur, the increase in pressure would be detected and the fast-acting valve would close within 25 msec, preventing damage to the Van de Graaff.

Calculations indicate that the shock wave should reach the fast-acting valve in approximately 10 msec, which is faster than the reaction time of the system. However, various sections of the beam tube act as baffles and tend to break up and slow down the shock wave. Those sections which have a baffling effect are a 1.5 cm diameter collimator, the four-way current monitor located immediately above the entrance window and a 2.5 cm diameter collimator located above the beam profile monitor. There are also sections of the beam tube containing "T" - junctions which house various instruments and provide a dead space into which the shock wave can expand, thus producing a diffusing effect.

In order to test the effectiveness of the fast-acting valve, taking into account the above parameters, the following procedure was carried out. A small known volume of helium was admitted into the vacuum system at the position of the thin foil entrance window and the amount of helium that escaped past the fast-acting valve measured with a helium sensitive detector. A measurement of the amount of helium reaching the detector with the fast-acting valve inhibited was compared with the amount of helium reaching the detector with the valve active. The results indicated that less than 0.1 per cent of the 10 cm^3 volume of helium escaped past the valve. Failures during actual experiments have shown the valve to be fast enough so that no increase in pressure is registered in the vacuum section of the Van de Graaff.

CHAPTER 4

PRODUCTION AND UTILIZATION OF $^{11}\text{CO}_2$

4.1 Introduction

The nuclear reaction $^{11}\text{B}(\text{p},\text{n})^{11}\text{C}$, used for the production of ^{11}C , was chosen for several reasons. The target material, B_2O_3 , is readily available and the reaction has a relatively high cross section. The only significant competing reaction, $^{18}\text{O}(\text{p},\text{n})^{18}\text{F}$, accounts for less than one per cent of the total activity.⁵⁸ Due to the high chemical reactivity of ^{18}F , it will combine with molecules in the target cell and not be collected with the $^{11}\text{CO}_2$.

The target material chosen was boron trioxide made from naturally occurring boron with a ^{11}B content of 80.22 per cent. The target was prepared by heating 1.0 gm of B_2O_3 to 500°C to melt it into an aluminum dish. After cooling, the B_2O_3 formed a glassy disc 2.7 cm in diameter and 0.3 cm thick. The energy loss of a beam of 6.0 MeV protons in boron is approximately 130 MeV/cm, thus the yield for the $^{11}\text{B}(\text{p},\text{n})^{11}\text{C}$ reaction can be considered a thick target yield.

The nuclear reaction $^{11}\text{B}(\text{p},\text{n})^{11}\text{C}$ has an effective Q value of approximately 4 MeV and a high total cross section with a large resonance at 6.0 MeV⁵⁹ (Figure 9). The amount of ^{11}C produced from this reaction can be calculated using Eq. 2.38:

$$\text{N}'_{\text{B}} \text{P}_{\text{B}} = \text{N}_A \text{N}_X \sigma (1 - e^{-P_B t}) \quad (4.1)$$

where

$$\begin{aligned} \text{N}_A &= \text{number of target molecules} \\ &= 2.2 \times 10^{20}, \end{aligned}$$

$$\begin{aligned} \text{N}_X &= \text{number of bombarding protons} \\ &= 6.24 \times 10^{12} / \mu\text{A} \cdot \text{cm}^2 \cdot \text{sec}, \end{aligned}$$

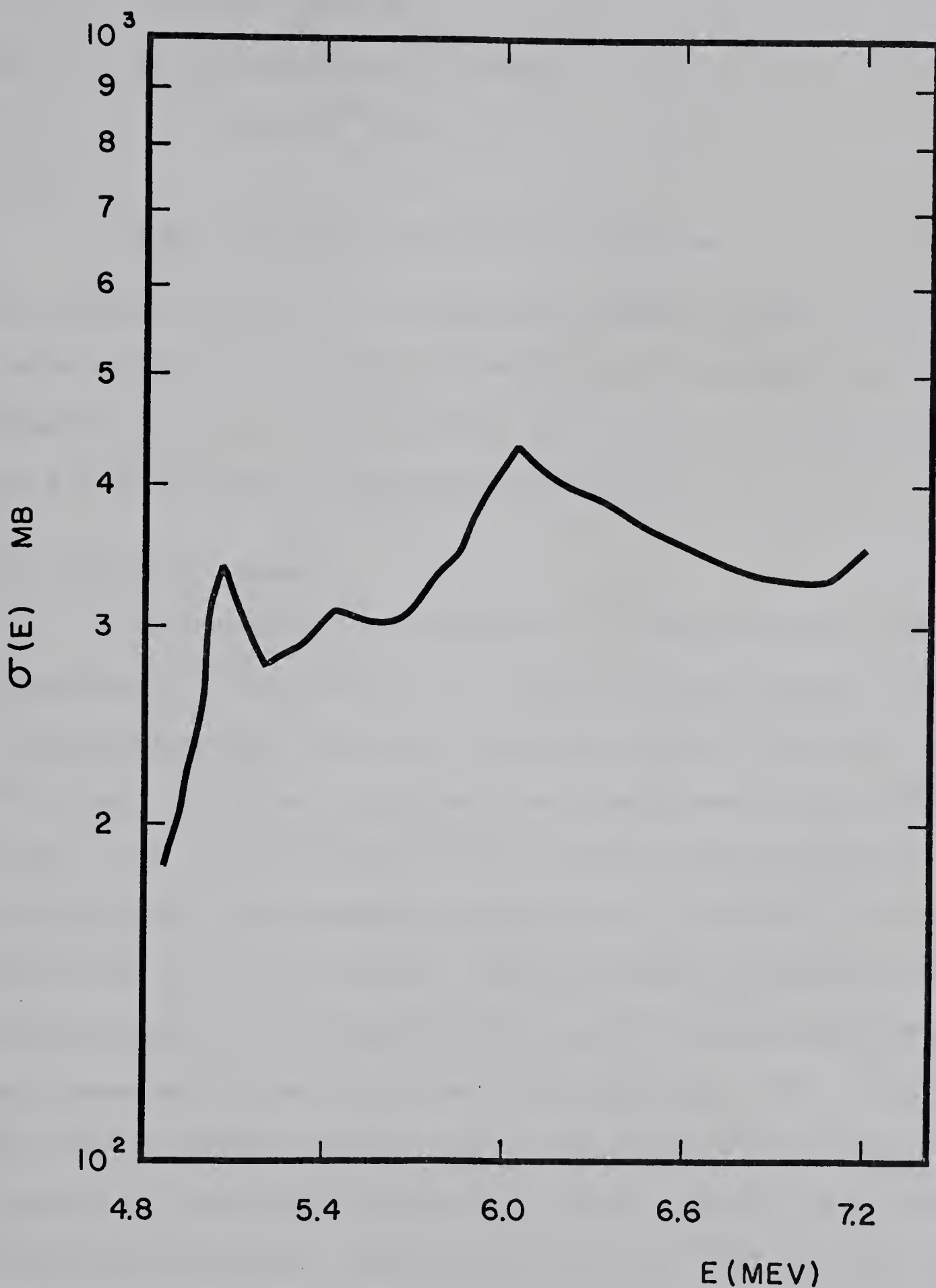
CROSS SECTION OF $^{11}\text{B}(\text{p},\text{n})^{11}\text{C}$ REACTION

FIGURE 9

$$\begin{aligned}\sigma &= \text{reaction cross section} \\ &= 4.00 \times 10^{-25} \text{ cm}^2, \\ \text{and } P_B &= \text{probability of } {}^{11}\text{C decay} \\ &= 5.78 \times 10^{-4}/\text{sec.}\end{aligned}$$

Thus,

$$N'_B P_B = 5.4 \times 10^8 (1 - e^{-5.78 \times 10^{-4} t}) / \mu\text{A} \cdot \text{sec} \quad (4.2)$$

The solution of Eq. 4. at $t = \infty$ gives the maximum activity of ${}^{11}\text{C}$ that can be produced: 14.6 mCi/ μA . After a bombarding time of one hour, or three half-lives of ${}^{11}\text{C}$, 12.9 mCi/ μA of ${}^{11}\text{C}$ will have been produced which is 87 per cent of the maximum yield value.

4.2 Production System

The system for the synthesis of ${}^{11}\text{C}$ -labelled carbon dioxide consists of a ${}^{11}\text{C}$ production cell, a gas flow control system, various chemical traps, and a collection and storage system (Figure 10). The ${}^{11}\text{C}$ production cell is a stainless steel chamber containing the B_2O_3 target. The target is located directly beneath the thin entrance foil which separates the atmospheric pressure in the production cell from the vacuum in the Van de Graaff. The B_2O_3 target is positioned so that protons emerging from the accelerator tube will interact with the target, producing ${}^{11}\text{C}$, and locally melt the B_2O_3 target. The ${}^{11}\text{C}$ produced will tend to combine with the oxygen in the target in an attempt to complete its outer shell of electrons. As the target is in a molten state during production, the resulting mixture of ${}^{11}\text{CO}$ and ${}^{11}\text{CO}_2$ will be released from the target.

The removal of the ${}^{11}\text{C}$ -labelled carbon monoxide and carbon dioxide from the site of production is accomplished by flowing helium

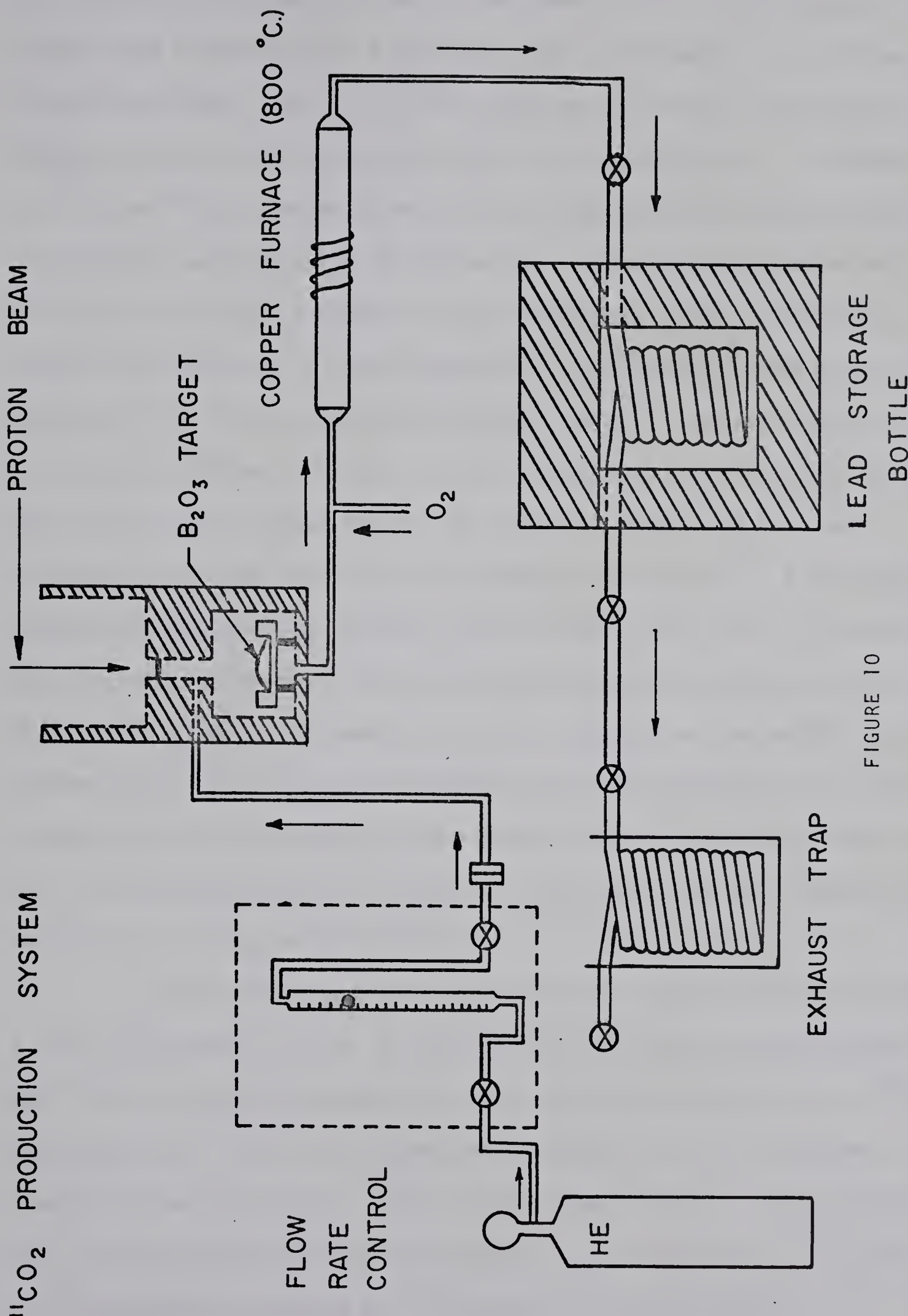


FIGURE 10

gas through the system at a controlled rate. Helium was chosen as a carrier gas because it has a relatively low cross section for proton induced reactions. Also, it is not affected by the low temperature regions of the collection system and is chemically inert. The amount of ^{11}CO and $^{11}\text{CO}_2$ carried from the B_2O_3 target to the trapping system is dependent upon the rate of helium flow. A gas control system was developed to provide a method of circulating the helium carrier gas through the system at a controlled rate. The control system (Figure 10) consisted of a double needle valve with a vernier control coupled to a flow meter. Valves at either end of the system provide shut-off control. The rate at which helium enters the system is controlled by a gas regulator providing an injection pressure of 0.63 kg/cm^2 . A millipore filter was installed in the gas line at a point just prior to the production cell to remove any foreign material having a diameter greater than than 0.45 microns. The complete gas flow system was then sealed to prevent the ^{11}CO or $^{11}\text{CO}_2$ from escaping into the atmosphere, and the system calibrated to provide a controlled helium flow rate variable from $0.1 \pm 0.05 \text{ ml/min}$ to $200 \pm 10 \text{ ml/min}$. The helium flow rate used in the collection of $^{11}\text{CO}_2$ was 100 ml/min .

The gas mixture leaving the production cell was found to have a $^{11}\text{CO}_2/^{11}\text{CO}$ ratio of 3:1. To obtain pure $^{11}\text{CO}_2$ from the gas stream, the ^{11}CO must either be removed from the system or converted into $^{11}\text{CO}_2$. The removal of ^{11}CO can be accomplished through the use of various chemical traps specific to ^{11}CO or through the selective freezing out of the desired product from the gas mixture. Its conversion to $^{11}\text{CO}_2$ can be accomplished by passing the ^{11}CO over CuO heated to 800°C .

The efficiencies of the various collection techniques were measured using a series of traps, and then counting the activity in each. The simplest method involved the preferential freezing out of $^{11}\text{CO}_2$ from the He, ^{11}CO and $^{11}\text{CO}_2$ mixture. The large difference in the freezing points of carbon dioxide and carbon monoxide, -78°C and -191°C respectively, aids in their separation. The selective removal of $^{11}\text{CO}_2$ from the gas mixture was accomplished by flowing the gas through a copper coil, 8 m long with a 1.7 mm bore cooled in a bath of isopentane chilled to -159°C. This method has an efficiency of about 90 per cent for the collection of $^{11}\text{CO}_2$, but does not utilize the ^{11}C in the carbon monoxide labelled molecules.

Another method for the collection of $^{11}\text{CO}_2$ involved the use of chemical traps to remove the $^{11}\text{CO}_2$ and ^{11}CO from the gas stream. The gas mixture was bubbled first through a solution of 1.0 M NaOH which removed the $^{11}\text{CO}_2$ and then through Ag_2O powder which removed the ^{11}CO . The chemical traps were found to have an efficiency of approximately 99 per cent, but again the activity in the ^{11}CO was not utilized.

To utilize the ^{11}C incorporated into ^{11}CO it was necessary to convert the ^{11}CO to $^{11}\text{CO}_2$ and then collect the resulting $^{11}\text{CO}_2$. The conversion of ^{11}CO to $^{11}\text{CO}_2$ may be accomplished by heating the gas mixture to 800°C in the presence of oxygen and the catalyst copper oxide. To aid in the conversion an electric furnace was constructed, the main body of which consisted of a quartz tube 15 cm long and 2.5 cm in diameter. The heating element was made from a 115 cm length of nichrome resistance wire which was first coiled and then wrapped around the center of the quartz tube. The coil was then packed in asbestos and a pyrex tube, 7.5 cm long, was used to cover the heating coil and

asbestos. The pyrex cylinder was wrapped with eight alternating layers of aluminum foil and fiberglass tape to provide thermal insulation. The catalyst (copper oxide) was packed into the central region of the quartz tube enveloped by the heating coil. Approximately 200 watts of power was applied to the heating coil to provide a temperature of 800°C.

Upon leaving the conversion furnace the He, O₂ and ¹¹CO₂ entered a 3 m copper coil. The coil was suspended in a cold bath of isopentane which froze out the ¹¹CO₂. The helium and oxygen in the gas mixture, with boiling points of -268.6°C and -183.0°C respectively, were not affected by the cold trap. Only the ¹¹CO₂ was removed.

Typically 50 mCi of ¹¹CO₂ was collected in the cold trap representing the major source of the residual radiation field involved in the production of ¹¹C. To provide effective shielding for the ¹¹CO₂ a lead container was designed which served as a means of safely transporting the radionuclide. The lead container was constructed with a wall thickness of 4.5 cm and a total mass of approximately 34 kg.

The effectiveness of this shielding was determined by comparing the dose-rate inside the lead container with that on the outside surface.

Calculations based upon a 50 mCi source of ¹¹CO₂ inside the lead container indicated that the dose-rate inside was 250 Rem/hr as compared with a dose-rate outside of 10 mRem/hr. The dose-rate at one meter from the lead container was 0.02 mRem/hr.

4.3 Analysis of ¹¹CO₂

Quantitative analysis of the ¹¹CO₂ was accomplished by monitoring the activity collected in the cold trap. The monitoring involved detection of the 511-keV gamma rays, resulting from the annihilation of

the positron emitted during the decay of ^{11}C , with a 7.6 cm x 7.6 cm Na(Tl) scintillation detector. The output pulse of the detector was fed, via a preamplifier and amplifier, into a single channel pulse height analyzer which accepted input pulses corresponding to gamma-ray energies between 485 keV and 535 keV. The output pulses of the analyzer were then fed into a scaler which provided a measure of the number of ^{11}C atoms that had decayed. The detection system was calibrated with a standard positron source (^{22}Na). After background subtraction it was possible to convert the number of events recorded by the scaler into the amount of activity collected and hence into the number of ^{11}C -labelled molecules collected in the storage container.

Two methods were used for the qualitative analysis. The energy spectrum of the radionuclide in the cold trap was measured with a Nuclear Data 180 multichannel analyzer. This provided a measure of the gamma-ray spectrum up to energies of 1.5 MeV. This spectrum was compared with that resulting from the decay of ^{11}C and served to indicate those radioimpurities whose decay resulted in the emission of gamma rays with energies differing from 511 keV. The results indicated that the radiation present arose only from 511-keV gamma rays.

A more detailed analysis of the constituents in the cold trap was necessary to reveal the amount of ^{11}CO and any non-radioactive contaminants present. To achieve this an Aero Vac 722 mass spectrometer was used to analyze the gas mixture: the instrument indicates the relative partial pressures of gases present in the system. The Aero Vac 722 mass spectrometer has a detection sensitivity of 1 part in 10^7 and may be used for the analysis of gaseous compounds having molecular weights between 1 and 100. A sample injection system was developed

that allowed direct sampling from the $^{11}\text{CO}_2$ storage coil so as to eliminate unnecessary contamination during the analysis.

Qualitative and quantitative analysis of the different recovery techniques was undertaken to determine the best method of $^{11}\text{CO}_2$ collection. An analysis of the gas collected in a liquid nitrogen trap, before any processing, revealed the $^{11}\text{CO}_2/^{11}\text{CO}$ ratio to be approximately 3:1. A sample of the gas mixture taken after it had passed through the copper furnace and was trapped in liquid nitrogen indicated a $^{11}\text{CO}_2/^{11}\text{CO}$ ratio of 100:1. An analysis of the gas having passed through the copper furnace and then trapped in the cold bath of isopentane revealed no ^{11}CO present, within the detection sensitivity of the mass spectrometer. The only other gases detected were a small quantity of water vapor, present in amounts of 100 times less than the $^{11}\text{CO}_2$, and the carrier gas, He.

As indicated by the above analysis, the recovery system which yielded the purest $^{11}\text{CO}_2$ content used the copper furnace to reduce the ^{11}CO to $^{11}\text{CO}_2$ and then collected the $^{11}\text{CO}_2$ in a cold bath of isopentane. Other recovery systems that have been reported⁶¹ use liquid nitrogen cold traps to recover $^{11}\text{CO}_2$, and hence trap small quantities of ^{11}CO and O_2 . The cold trap of isopentane at -159°C operates above the liquification temperatures of these gases, thereby permitting the collection of a purer sample of $^{11}\text{CO}_2$.

4.4 Utilization of $^{11}\text{CO}_2$ in Lung Function Studies

In lung and heart diseases there may be marked changes in the distribution of gas and blood to the lungs. The changes can cause widespread alterations in bodily function and can be of clinical importance. Often the physiological and/or anatomical anomalies can be

detected by clinical examination and with the aid of radiography, but these methods of gross evaluation may be misleading and fail to detect small changes in local blood flow and gas distribution. With more complicated radiological evaluation (e.g. bronchography, tomography or pulmonary angiography) anatomical changes in different regions of the lungs can be detected, but the methods do not give a measure of local physiological conditions.

The use of radioactive gases have made the study of regional lung function much simpler. Xenon-133 was one of the first radioactive gases to be used,⁶² but initially resulted in low precision measurements of local ventilation and so was of limited value. However, the technique of using ¹³³Xe in the assessment of regional lung function has since improved and it is now used routinely in measurements of regional ventilation and perfusion (blood flow) of the lung.^{63,64} As ¹³³Xe is a nonphysiological gas there was interest in labelling physiological respiratory gases - oxygen, carbon dioxide and nitrogen.^{65,66} These gases have been used in pulmonary function studies in the form of ¹¹C-labelled CO and CO₂,⁶⁷⁻⁶⁹ ¹³N-labelled N₂⁷⁰ and ¹⁵O-labelled CO, CO₂ and O₂.⁷¹⁻⁷⁴

The advantages of radioactive gases used to make regional assessments of ventilation and blood flow, without discomfort to the patient, needs no elaboration. Tests require the simplest of manoeuvres from the patients, with breath holding the only deviation from physiological conditions.

A technique for measuring regional perfusion and ventilation in the lung using a radioactive gas, such as ¹¹CO₂, that is taken up by the lung is shown in Figure 11. The subject inhales a single breath of gas and holds his breath for 10 to 15 sec. Scintillation counters arranged

USE OF A RADIOACTIVE GAS IN REGIONAL LUNG FUNCTION STUDIES

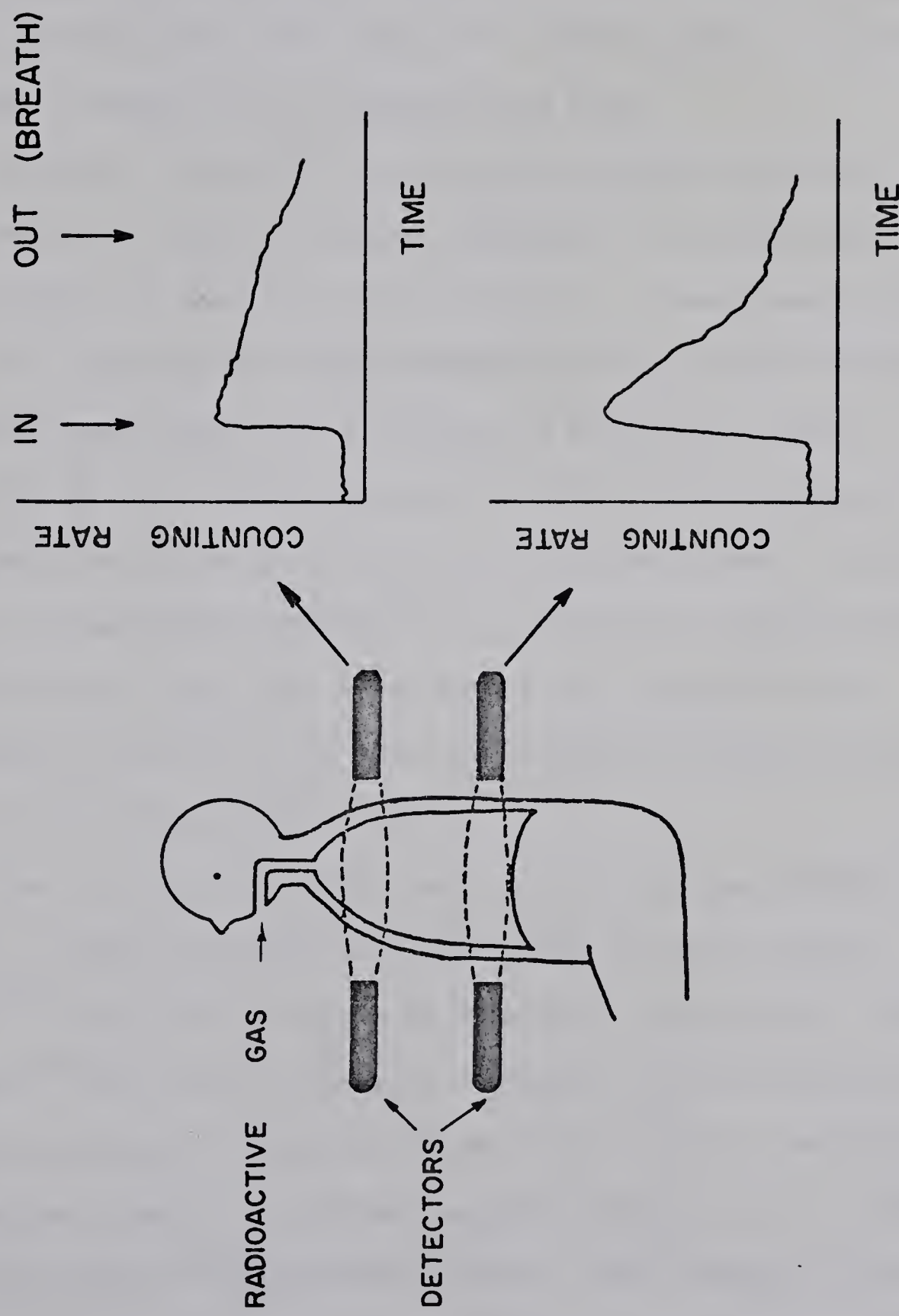


FIGURE 11

anteriorly and posteriorly to the chest record the activity of the gas in well-defined volumes of the lung between the counters. On inspiration, radioactive gas enters the counting field, therefore there is an increase in the counting rate that is related to the ventilation of the particular region of the lung being examined. During the short breath-holding period, radioactive gas is removed from the counting field by pulmonary blood: the fall of the counting rate or "clearance rate" yields a measure of the regional blood flow.

Pulmonary diseases⁷⁵ such as asthma, chronic bronchitis, and emphysema have the effect of causing a decrease in the number of alveoli available to take part in gas exchange. A measurement of the activity in a region of the lung displaying one of the above respiratory diseases would show up as a decrease in the initial rise of activity (Figure 12). Other pulmonary disorders such as pulmonary embolism restrict the amount of blood perfusing the alveoli. Such an effect is noticeable when monitoring the activity of a region of the lung demonstrating a decreased blood flow as the initial rise in activity does not decrease with time, but remains relatively constant during the test interval (Figure 12).

The study of radioactive gases in regional lung studies at the University of Alberta is facilitated by a radiospirometry system developed^{76,77} within the Division of Biomedical Engineering. This system uses ¹³³Xe for the measurement of regional lung ventilation and perfusion in patients and animals and has been adapted to use ¹¹CO₂ as the radioactive tracer. The system comprises sixteen, 2.54 cm diameter x 1.27 cm thick NaI(Tl) scintillation counters, eight mounted posterior to and eight mounted anterior to the chest (Figure 13). Each posterior

SCHEMATIC DIAGRAM OF REGIONAL VENTILATION AND
PERFUSION MEASUREMENTS OF NORMAL AND
ABNORMAL LUNG CONDITIONS

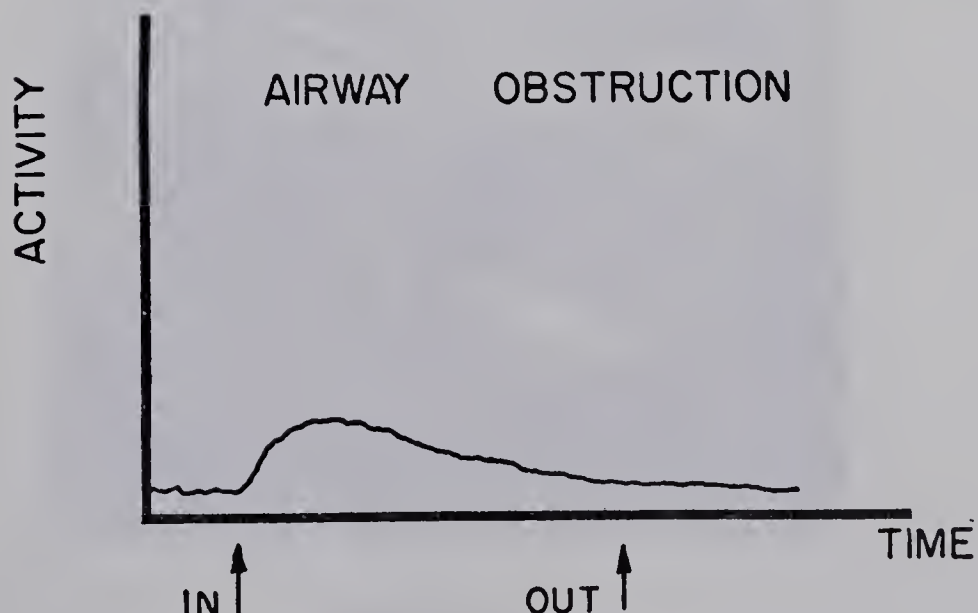
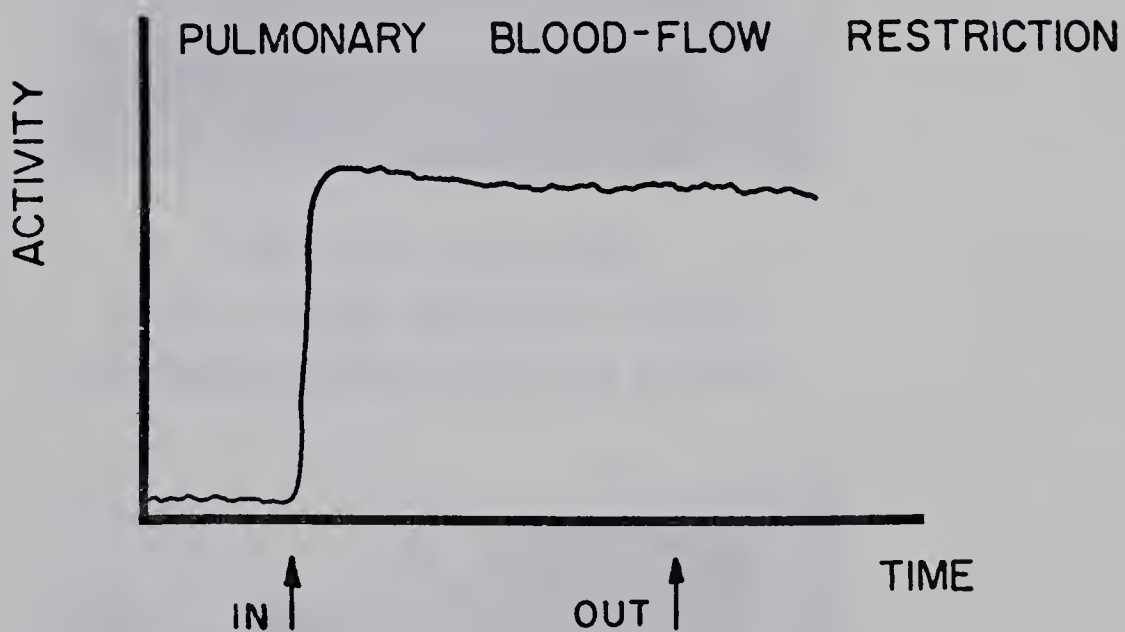
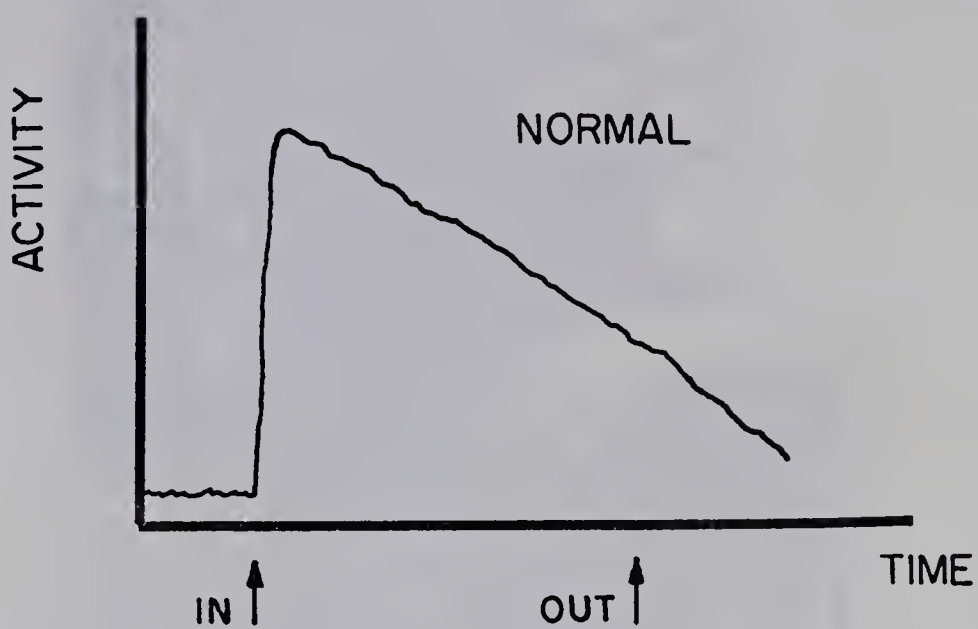
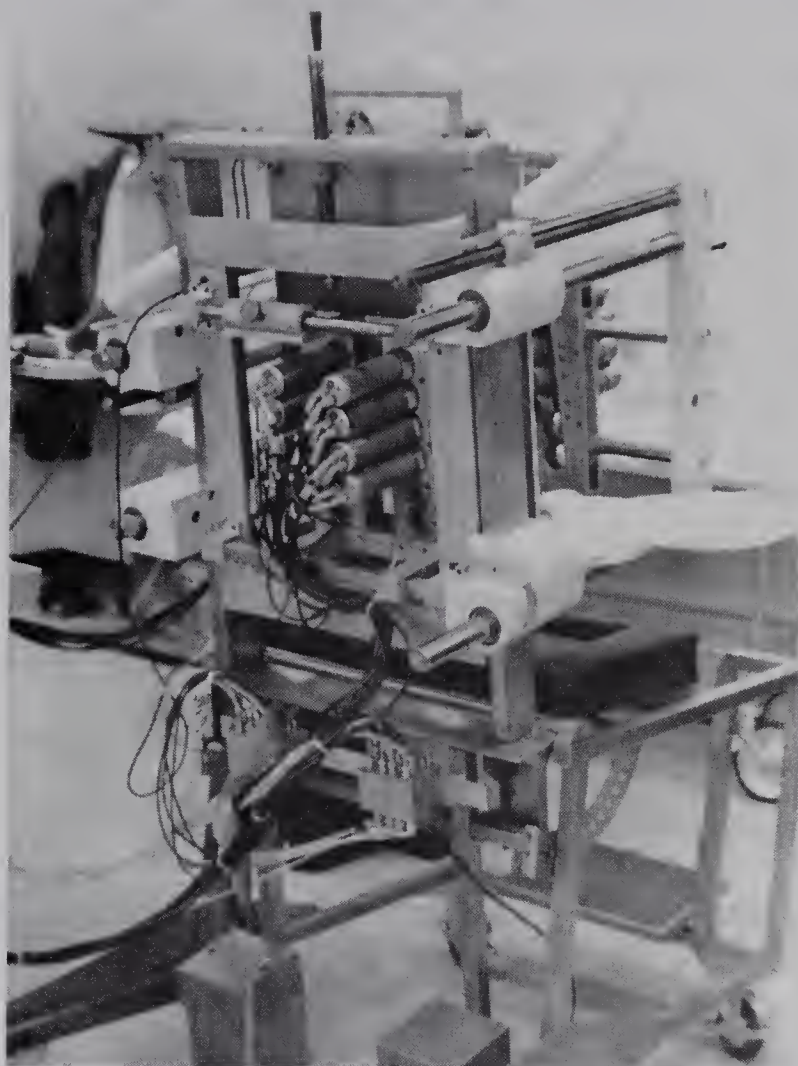


FIGURE 12



REAR AND SIDE VIEWS
OF 16 - PROBE DETECTION SYSTEM
FOR REGIONAL LUNG FUNCTION STUDIES

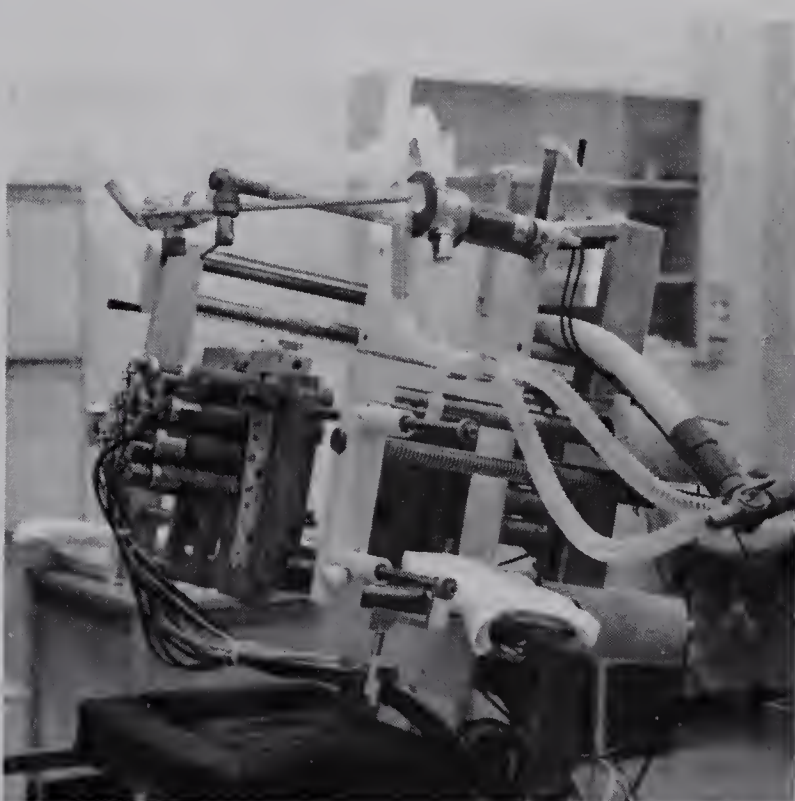
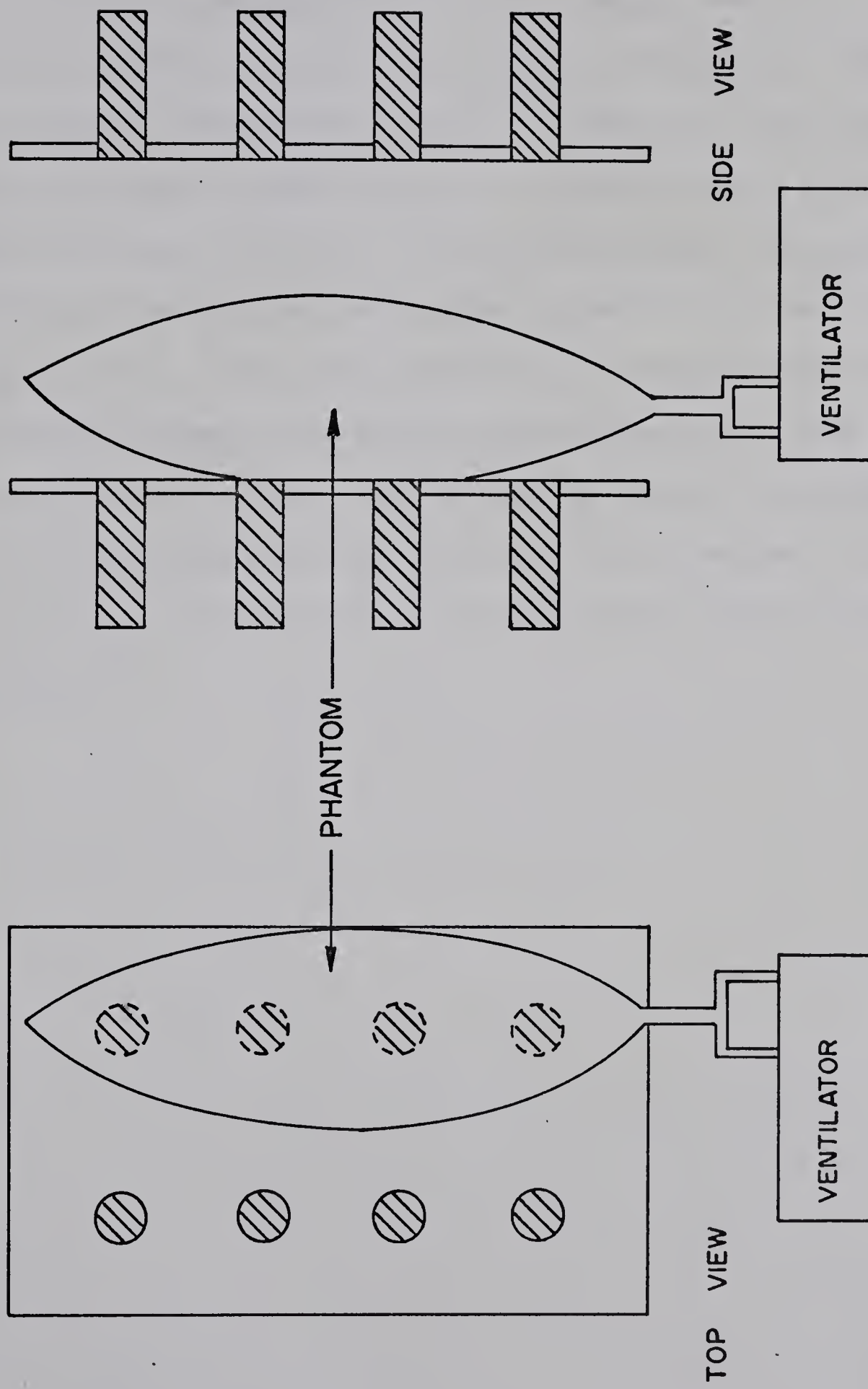


FIGURE 13

detector is paired with its corresponding anterior detector to form a colinear pair. Four pairs of detectors are mounted over each lung so that each detector pair views a different region. The output signals from each detector of a colinear pair are summed by the preamplifier. The output of the preamplifier is then passed to a linear amplifier and then through a single channel analyzer which provides an output pulse for those input pulses corresponding to a 511-keV gamma ray emitted during positron annihilation. The data from each single channel analyzer is fed into a scaler which records the number of pulses from the particular scaler for specified time intervals. The information from each scaler is transferred by a CAMAC dataway system to a Hewlett-Packard 2100A computer system for analysis and storage. This system permits on-line data processing and display.

To test the radiospirometry system, a phantom was constructed which consisted of a two-liter air bag used to simulate a lung. The phantom was located over one row of detectors and then attached to a ventilator (Figure 14). The phantom was ventilated with room air to simulate the ventilation of a test animal. At the end of an expiration cycle, corresponding to the functional residual capacity of the test animal, $^{11}\text{CO}_2$ was introduced into the phantom. This was followed by the inspiration cycle of the ventilator to wash the $^{11}\text{CO}_2$ into the phantom and inflate it. At the end of inspiration, corresponding to the inspiratory capacity of the test animal, the ventilator was shut off for fifteen seconds to simulate breath holding. At the end of this time the ventilator was switched on allowing the ventilation cycle to continue, with the expired $^{11}\text{CO}_2$ collected in an exhaust system. The results of tests with the phantom indicated that approximately 350 μCi of $^{11}\text{CO}_2$

SCHEMATIC DIAGRAM OF PHANTOM STUDY



■ - NaI(Tl) DETECTOR

FIGURE 14

should be administered to achieve a count of 5,000 cps for each detector pair.

It was planned to further test this system by measuring regional ventilation and perfusion in dogs. However, due to an accident with the Van de Graaff such a test was not possible. The results on similar measurements of dogs^{78,79} reveal that the perfusion per unit lung volume is nearly the same for upper and lower regions of the lung in the supine position. In the erect position, the perfusion per unit lung volume for the lower region is greater than that for the upper region. When in the supine position, an anteroposterior perfusion gradient is also present. The relative ventilation in the lobes of the dog is also effected by posture and is markedly reduced in the upper region of the lung when the animal is tilted from the supine to the upright position. Results similar to these have been shown in normal human subjects.⁸⁰

CHAPTER 5
PRODUCTION OF ^{18}F -LABELLED URACIL

5.1 Introduction

Fluorine-18 was produced through the deuteron bombardment of ^{20}Ne and used to label uracil, a pyrimidine base. Although 2'-deoxyuridine will ultimately be the labelled compound, uracil was used in its place because the labelling process is the same for both molecules, and uracil is more readily available and less expensive than 2'-deoxyuridine. Although several other nuclear reactions^{81,82} have been used to produce ^{18}F , the $^{20}\text{Ne}(\text{d},\alpha)^{18}\text{F}$ reaction was chosen because of its relatively high production cross section (Figure 15) and the fact that there are no significant competing reactions when the incident deuteron energy is less than 9 MeV.^{83,84}

The target material was composed of naturally occurring neon gas in which the ^{20}Ne content is 90.92 per cent. The total thickness of the target was 26 cm, which corresponds to a 3.4 MeV energy loss for the 6.5 MeV deuterons that were used in the production. The threshold for the $^{20}\text{Ne}(\text{d},\alpha)^{18}\text{F}$ reaction is given by Eq. 2.23 as

$$\begin{aligned} Q_{\text{Eff}} &= Q_{\text{Thr}} + Q_C \\ &\approx 2 \text{ MeV.} \end{aligned} \tag{2.23}$$

The neon target may therefore be considered a thick target for the purpose of calculating the yield. From Eq. 2.38, the amount of ^{18}F produced at any time t via the $^{20}\text{Ne}(\text{d},\alpha)^{18}\text{F}$ reaction is

$$N'_B = N_A N_X \sigma (1 - e^{-P_B t}) \tag{5.1}$$

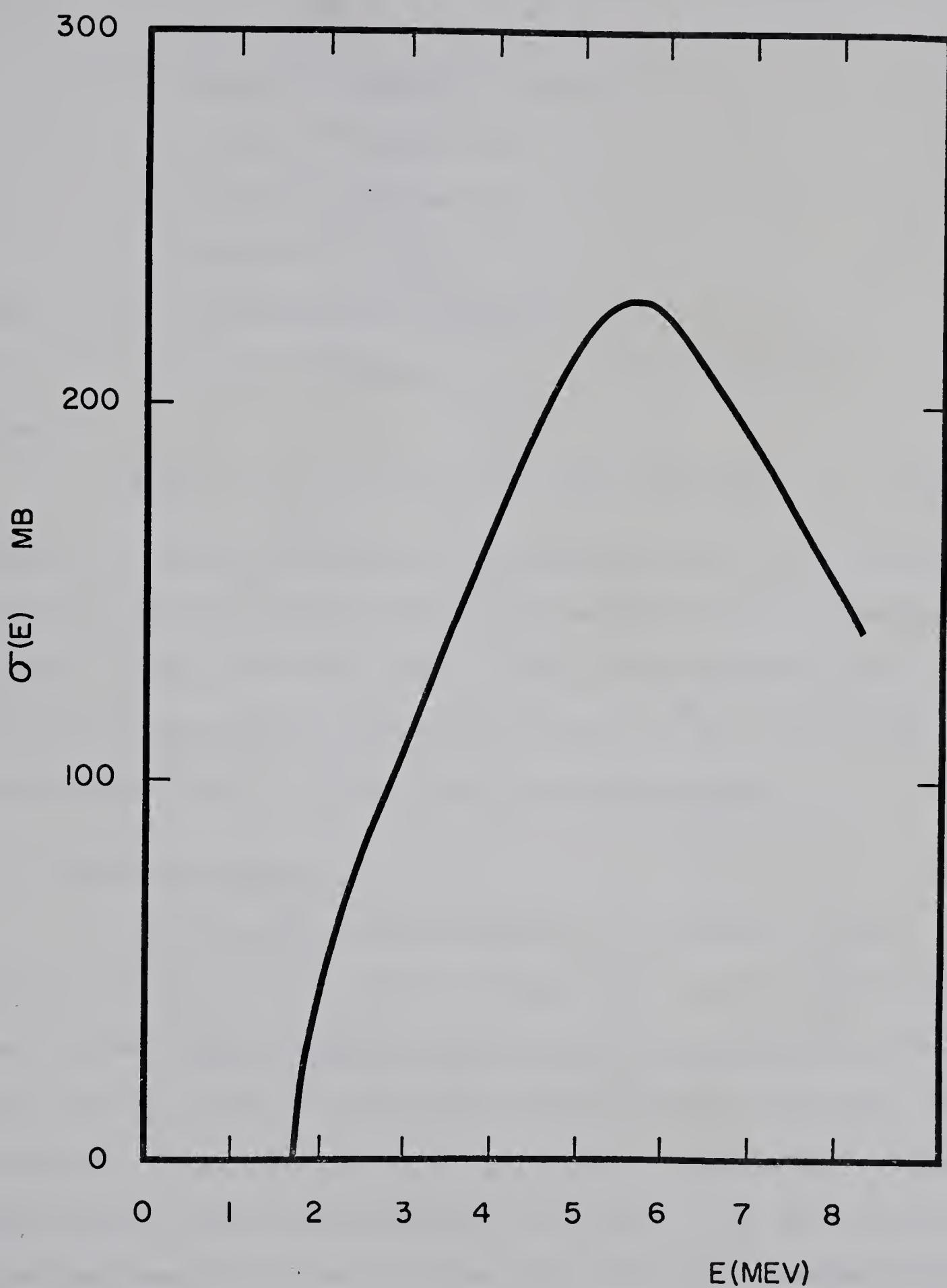
CROSS SECTION OF $^{20}\text{Ne}(\text{D},\alpha)^{18}\text{F}$ REACTION

FIGURE 15

where N_A = number of target nuclei
 $= 2.1 \times 10^{20}$,

N_X = number of bombarding deuterons
 $= 6.24 \times 10^{12} / \mu\text{A} \cdot \text{cm}^2 \cdot \text{sec}$,

σ = reaction cross section
 $= 2.25 \times 10^{-25} \text{ cm}^2$,

and P_B = probability of ^{18}F decay
 $= 1.05 \times 10^{-4} / \text{sec}$.

Thus,

$$N'_B P_B = 2.95 \times 10^8 [1 - e^{-(1.05 \times 10^{-4} t)}] / \mu\text{A} \cdot \text{sec} \quad (5.2)$$

where t is measured in seconds. The solution of Eq. 5.1 at $t = \infty$ provides the maximum yield of ^{18}F that may be produced with an incident deuteron energy of 6.5 MeV: $8 \text{mCi}/\mu\text{A}$. After an irradiation time of 5.5 hrs, corresponding to three half-periods of ^{18}F , $7 \text{ mCi}/\mu\text{A}$ will have been produced which is 87 per cent of the maximum yield.

5.2 Production System

The system for the production of ^{18}F consists of a gas target production cell, a reaction vessel where uracil is fluorinated and a closed loop circulation system. The ^{18}F production cell consists of a $26 \text{ cm} \times 1.5 \text{ cm}$ I.D. stainless steel tube which contains the ^{20}Ne target gas. The production cell is situated directly beneath the thin foil entrance window which separates the vacuum of the Van de Graaff from the atmospheric pressure of the neon gas target. Leading directly from the production cell is a stainless steel reaction vessel containing uracil (Figure 16). After the production of ^{18}F is completed a peristaltic pump circulates the $\text{Ne}-^{18}\text{F}$ gas mixture from the

FLUORINE - 18 PRODUCTION SYSTEM

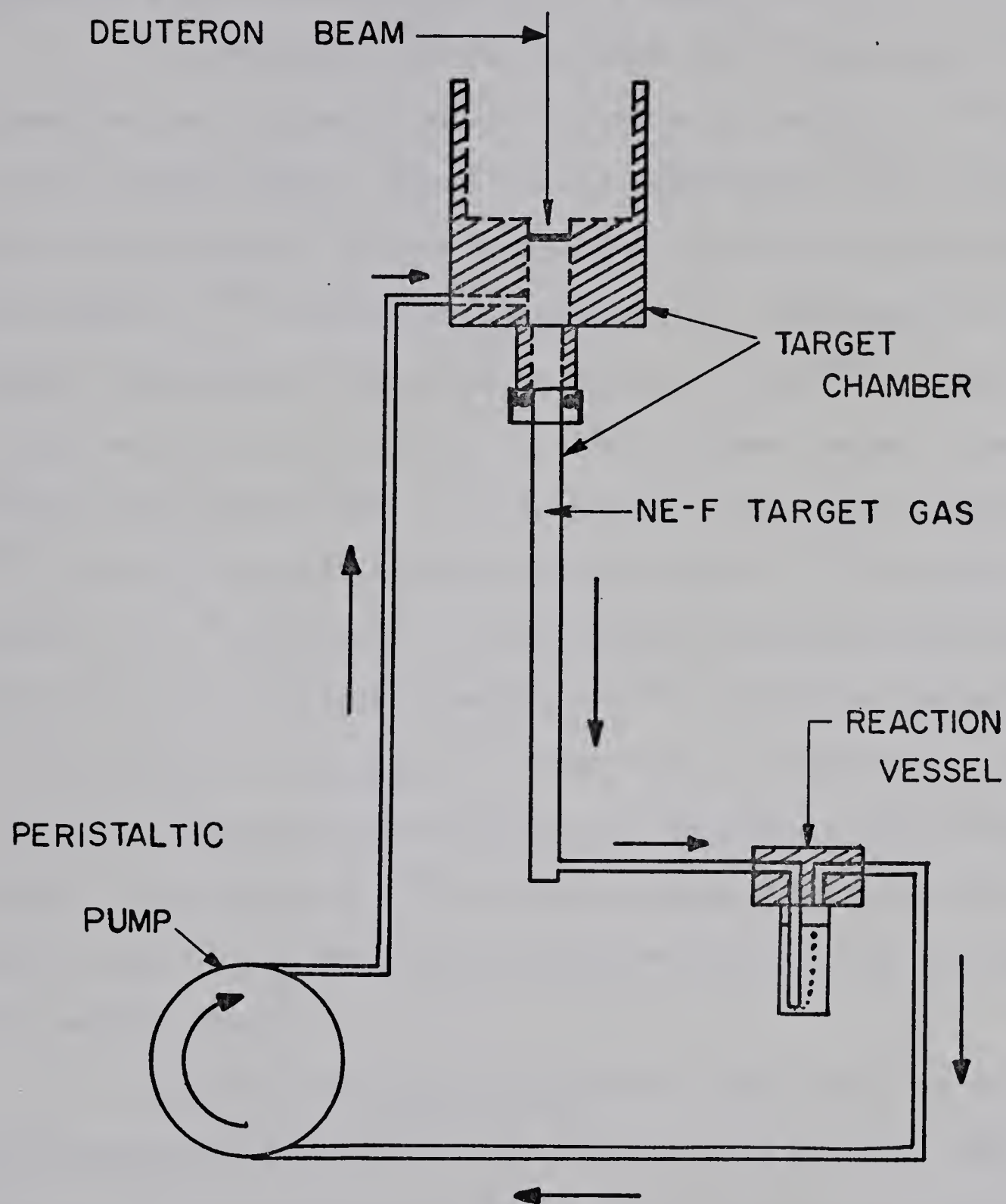


FIGURE 16

production cell through the reaction vessel where an exchange reaction takes place to label the uracil with ^{18}F (Figure 17).^{85,86}

In the initial experiments involving the production of ^{18}F , phenol was used instead of uracil to measure the amount of ^{18}F available to the reaction vessel. Phenol readily combines with ^{18}F , removing it from the gas stream, and thus providing a quantitative measure of the amount of ^{18}F reaching the reaction vessel. The results of these studies indicated that more than 99 per cent of the ^{18}F remained bound to the walls of the production cell after the neon gas was circulated through the reaction vessel. In an attempt to increase the amount of ^{18}F reaching the reaction vessel a small amount of ^{19}F was added to the system, to a $^{19}\text{F} : ^{20}\text{Ne}$ ratio of 1:9, thereby fluorinating the production cell walls and reducing the tendency of ^{18}F to bind with the walls as it was produced. The gaseous ^{19}F also acted as a carrier for the ^{18}F to keep it in gaseous form and aid in its transport to the reaction vessel. The addition of ^{18}F to the gas mixture resulted in 10 ± 5 per cent of the ^{19}F that was produced being incorporated into the phenol in the reaction vessel.

Several other methods were used to label uracil in an attempt to incorporate more of the ^{18}F into the labelling process. One method employed lithium fluoroborate (LiBF_4) as the fluorinating agent.^{87,88} This process involved two steps, first the labelling of LiBF_4 with ^{18}F and then the transfer of the ^{18}F from $\text{LiB}^{18}\text{F}_4$ to uracil. Fluorine-18 was produced by the same nuclear reaction on neon gas, but in this case no ^{19}F was added to the gas mixture resulting in the ^{18}F being incorporated into the walls of the production cell. After the radionuclide production was finished, the walls of the production cell were washed

URACIL LABELED WITH $^{18}\text{F}_2$ GAS

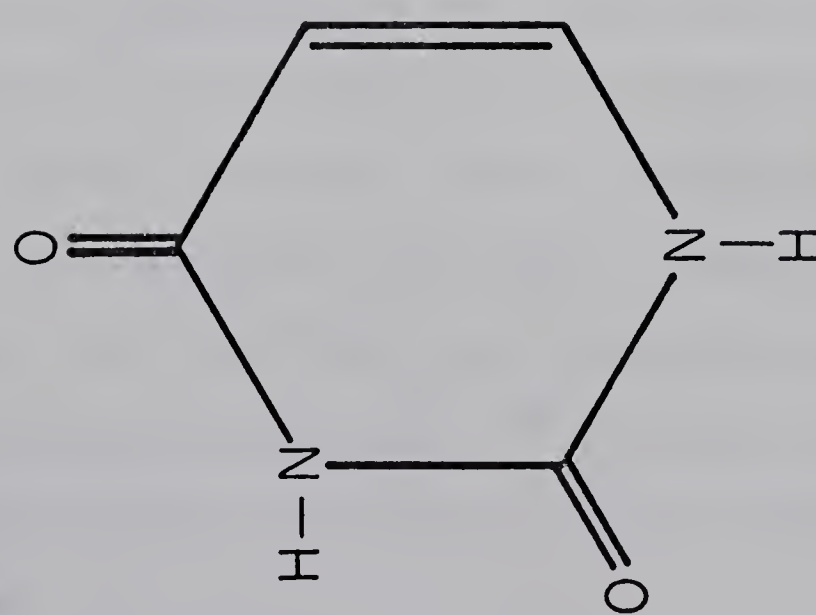
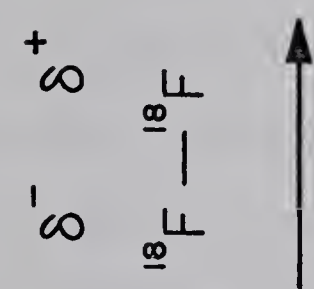
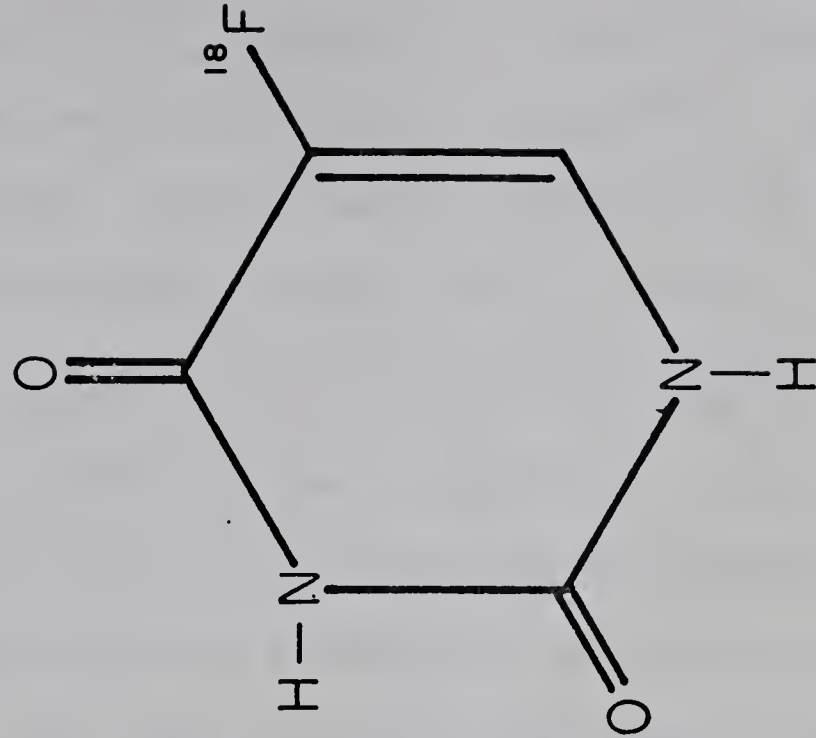


FIGURE 17

with 1.0 gm of LiBF₄ dissolved in 5.0 ml of triple distilled water.

An exchange reaction took place with the ¹⁹F in LiBF resulting in ¹⁸F-labelled LiBF₄. In this reaction, approximately 50±10 per cent of the ¹⁸F produced was incorporated into the solution of LiBF₄.

In order to accept the ¹⁸F from LiB¹⁸F₄, it was necessary to chemically prepare the uracil (Figure 18). Uracil was first labelled in the five position with bromine and then dissolved in a mixture of ammonia and ethanol to yield uracil with an amino group at the five position. The 5-amino uracil was then added to a solution of NaNO₂ and HCl: the resulting reaction formed a diazonium salt at the five position of uracil. The solution of ¹⁸F-labelled LiBF₄ and distilled water was then added to the uracil diazonium salt and through an exchange reaction 5-fluoro-uracil was produced.

Another method for the labelling of uracil with ¹⁸F involves the potassium salt potassium fluoride (KF) as the fluorinating agent. As before, ¹⁸F was produced and allowed to bind with the production cell walls. At the conclusion of the radionuclide production the walls of the production cell were washed with KF dissolved in triple distilled water and an exchange reaction took place between the ¹⁸F bound to the walls and the ¹⁹F in the potassium salt. Washing the walls with the solution of KF for two minutes removed approximately 70±10 per cent of the ¹⁸F. This solution was then added to 5-bromo-uracil dissolved in crown ether. The crown ether caused the disassociation of the K¹⁸F, releasing the highly nucleophilic ¹⁸F into the solution, where it displaced the bromine atom bound to uracil to produce 5-fluoro-uracil (Figure 19).

URACIL LABELED WITH $\text{LiB}^{18}\text{F}_4$

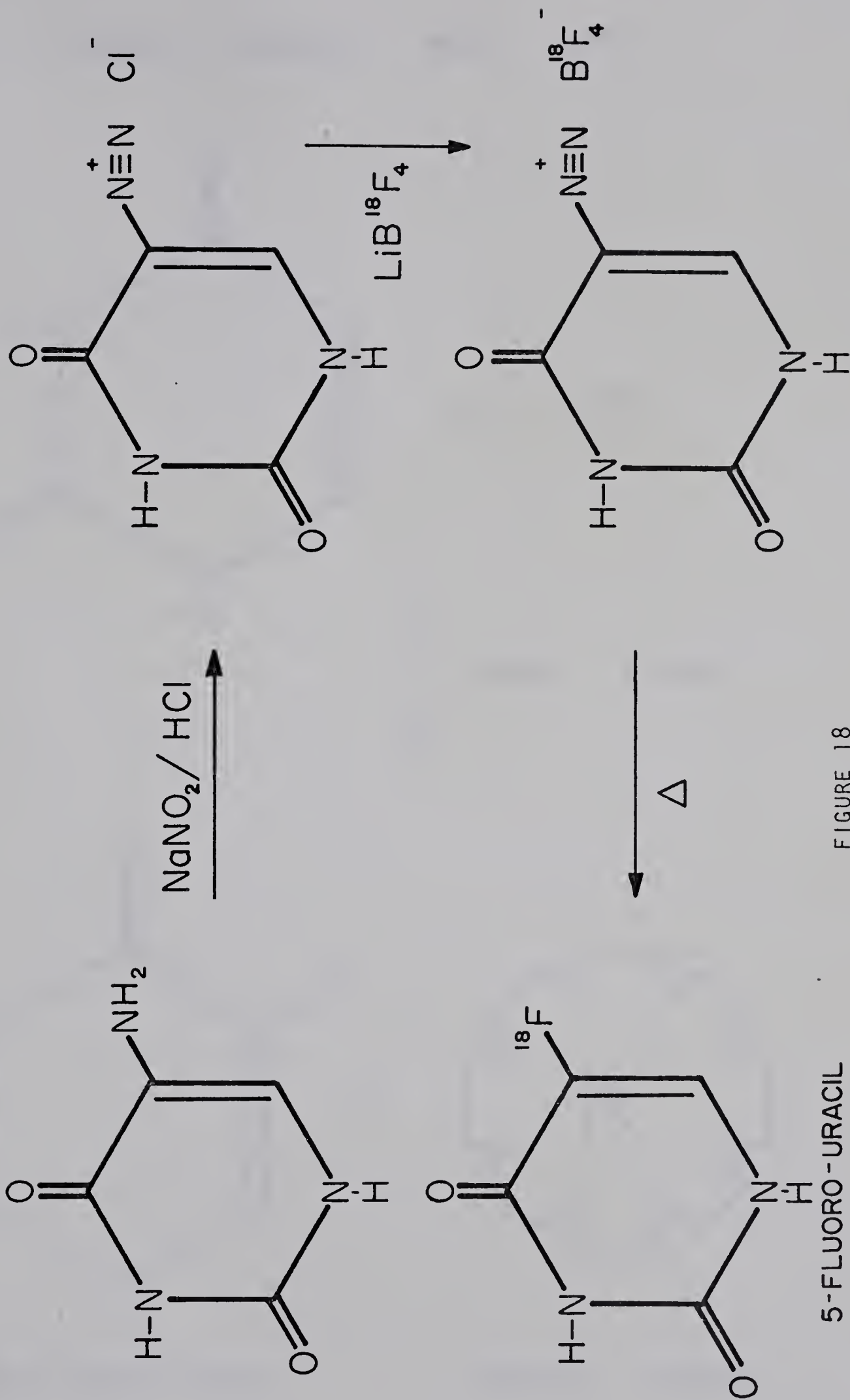
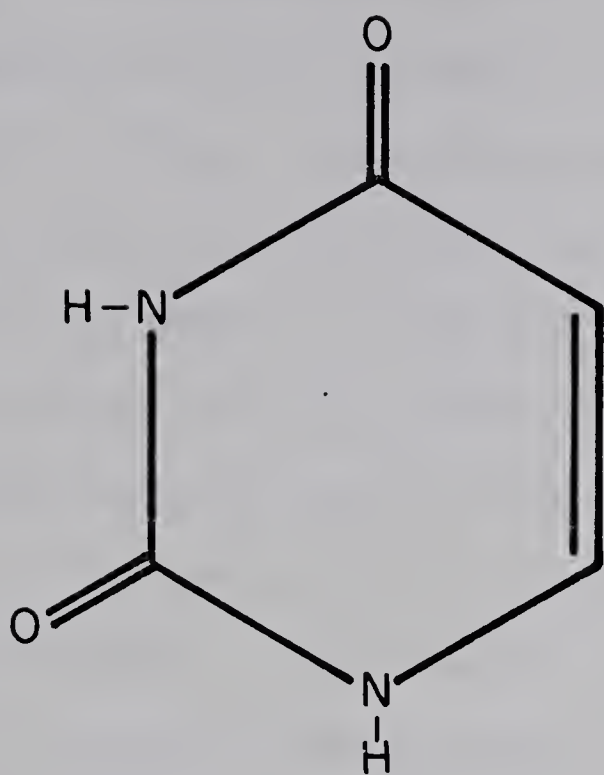


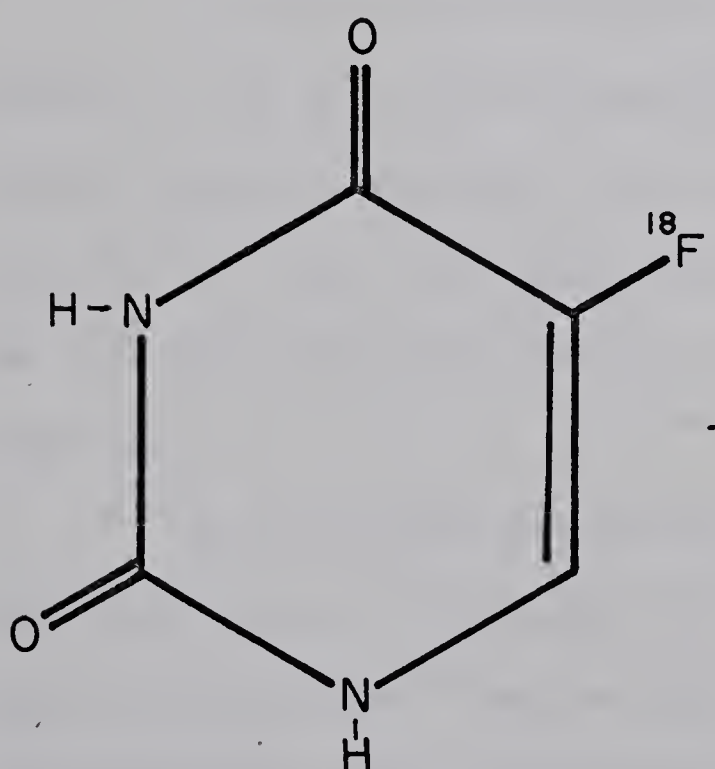
FIGURE 18

URACIL LABELED WITH $K^{18}F$

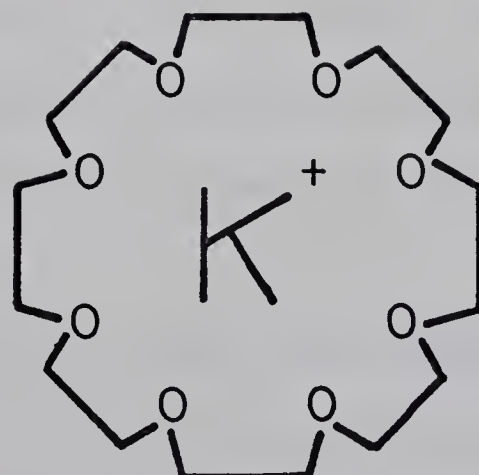


+ $K^{18}F$

CROWN ETHER



5-FLUORO-URACIL



CROWN ETHER

FIGURE 19

5.3 Analysis of ^{18}F -Labelled Compounds

The quantitative analysis of 5-fluoro-uracil and the various intermediates used in its preparation was similar to the quantitative analysis of $^{11}\text{CO}_2$. The same apparatus, a NaI(Tl) scintillation detector and associated electronics, was used to indicate the number of ^{18}F atoms in the sample. The results of an analysis of the quantity of ^{18}F in the production cell, a measure of the total amount of ^{18}F that was produced, agreed to within 10 per cent of the predicted theoretical value. This system was also used to indicate the relative efficiencies of the different methods used to remove the ^{18}F from the production cell in preparation for labelling the uracil. Of the various methods used to prepare an intermediate for labelling, the technique using the KF ion exchange reaction appeared to be the most successful, with 70 ± 10 per cent of the ^{18}F that was produced being incorporated into KF.

A crude qualitative analysis of radioactive contaminants present in the sample was accomplished with a Nuclear Data 180 multi-channel analyzer, employing techniques similar to those used in the analysis of $^{11}\text{CO}_2$. After background subtraction, analysis indicated the only gamma radiation present below 1.5 MeV resulted from 511-keV gamma rays.

To achieve greater sensitivity in the qualitative analysis of the various samples, a necessity for medical applications, high pressure liquid chromatography⁸⁹ may be used. This technique also permits the rapid separation and purification of the sample. The sample to be analyzed is introduced into the chromatographic column at pressures up to 420 kg/cm^2 . The different components in the sample are separated in the chromatographic column on the basis that each

substance has different absorption characteristics. There are two different methods used to detect and identify the different components as they emerge from the column. One involves a class of detectors, called bulk property detectors, that measure changes in the overall properties of the mobile phase. The other method, which is more sensitive, responds to physical properties of the solute. It is expected that the purification and elution of 5-fluoro-uracil will take less than fifteen minutes employing high pressure liquid chromatography.

5.4 Utilization of 5-Fluoro-2'-Deoxyuridine in Oncology

Uracil was chosen to be labelled with ^{18}F in the initial experiments because it was more readily available than 2'-deoxyuridine, and easier to work with. The procedures that were used to label uracil remain the same for the ^{18}F labelling of 2'-deoxyuridine. The nucleoside 2'-deoxyuridine is composed of uracil joined by an N-glycosyl linkage to the pentose sugar, deoxyribose. The linkage is between the nitrogen atom one of uracil and the carbon atom one of deoxyribose.⁹⁰ A diagram of the molecule and the numbering system of its various constituents is shown in Figure 20.

The nucleoside, 2'-deoxyuridine, is actively transported into the cell where it may be incorporated into DNA, through a salvage pathway into RNA, or converted to thymine.⁹¹ If 2'-deoxyuridine is labelled with ^{18}F its usual cellular function will be changed. Present research with labelled 2'-deoxyuridine indicates that it is not incorporated in DNA and only small amounts incorporated into RNA.⁹² Most of the labelled nucleoside is converted to 5- $^{18}\text{F}-2'$ -deoxyuridine monophosphate which may then combine with thymidylate synthetase in a reaction where

CHEMICAL STRUCTURE OF 5 - FLUORO - 2' - DEOXYURIDINE

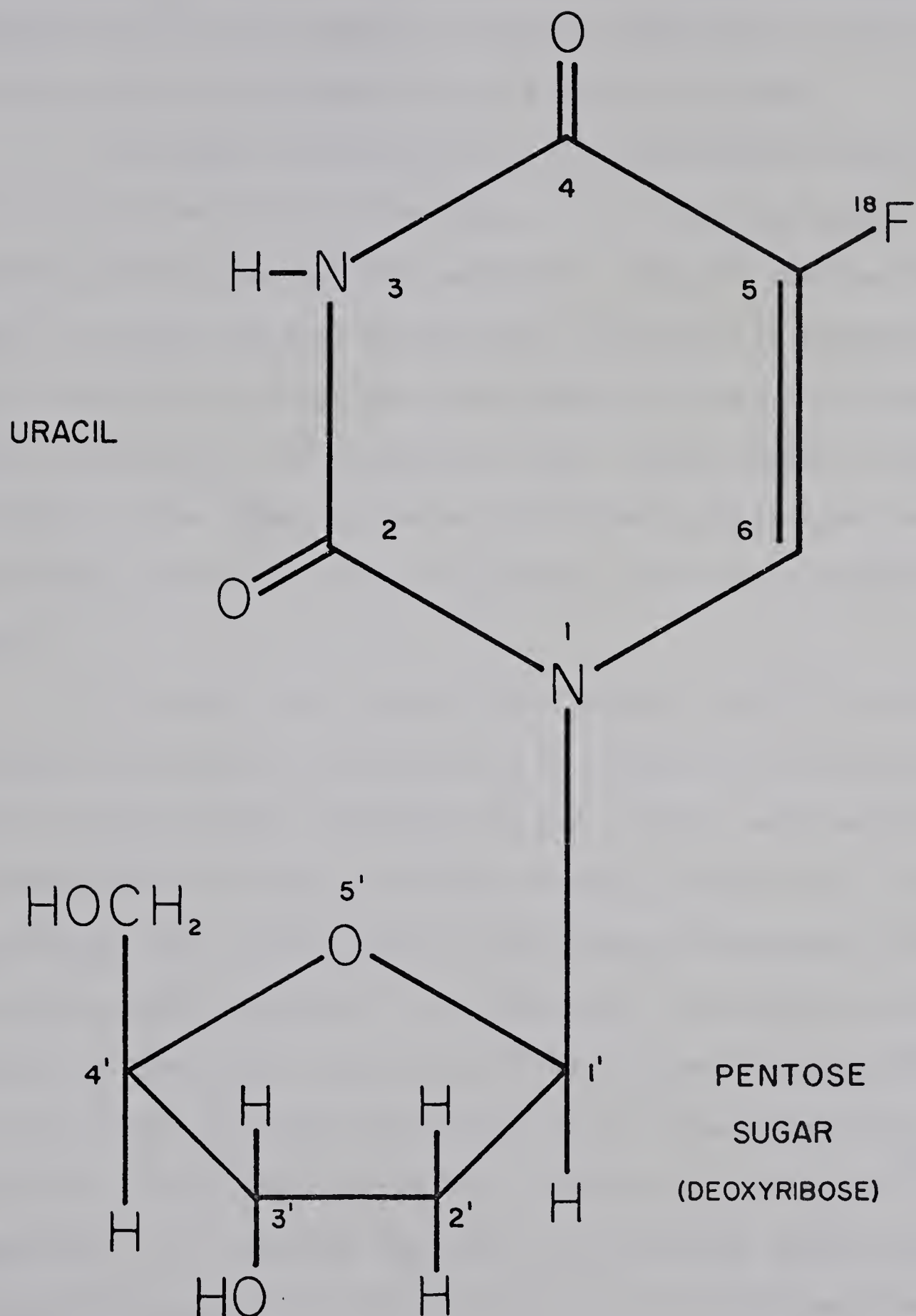


FIGURE 20

2'-deoxyuridine monophosphate is normally converted to deoxythymine monophosphate. However, because the 2'-deoxyuridine monophosphate is labelled with ^{18}F , the enzymatic reaction is inhibited and the labelled 2'-deoxyuridine monophosphate remains bound to the enzyme.

The uptake and utilization of 2'-deoxyuridine by cells can be used to selectively label those cells, such as cancerous cells, requiring large amounts of that nucleoside. Cancer⁹⁷ results from a change in certain cells of the body that allows them to disregard normal growth limits and no longer obey the feedback controls that normally stop cellular growth and reproduction after a given number of cells have developed. These cells experience a much faster growth rate than the surrounding normal cells and must synthesize more RNA to maintain their growth.

To utilize the 2'-deoxyuridine labelled with ^{18}F in diagnostic oncology, the labelled nucleoside will be injected into the blood stream where it will circulate throughout the body. Those cells requiring 2'-deoxyuridine for their growth will actively transport the 5-fluoro-2'-deoxyuridine into the cell where it will become incorporated in RNA by a salvage pathway and bound to an enzyme used in the synthesis of thymine, thymidylate synthetase. After most of the labelled 2'-deoxyuridine has been absorbed by the body the activity of the ^{18}F at the tumor site will be obtained through positron imaging to locate regions of high ^{18}F concentration. It is expected that much of the labelled uridine will be absorbed by the gastro-intestinal tract, as it is continuously building enzymes for the digestion and absorption of nutrients. Tumors present in the abdominal area will therefore be difficult to detect.

However, the localization of tumors away from the abdominal area, such as those encountered in breast cancer, will be possible using this technique. From measurements of the uptake of ^{18}F , it will be possible to determine the extent of the tumor. As ^{18}F has a half-life of only 110 minutes, it will be possible to repeat the imaging procedure at frequent intervals, thereby determining the effectiveness of the treatment.

REFERENCES

1. E. Freedman and C.C. Dundon, Medical Physics, Vol. 1, O. Glasser (ed), Year Book Publishers Inc., Chicago, Ill., p 1401, 1944.
2. G.L. Brownell and R.J. Shalek, Physics Today 23, p 32, 1940.
3. P.F. Hahn, J.P.B. Goodell and C.W. Sheppard, R.O. Cannon and H.C. Francis, J. of Lab. and Clin. Med., 32, p 1442, 1947.
4. R.D. Evans, Medical Physics, Vol. 1, O. Glasser (ed), Year Book Publishers Inc., Chicago, Ill., p 643, 1944.
5. P.F. Hahn, R.F. Ross, W.F. Bale, W.M. Balfour and G.H. Wipple, J. Exp. Med. 75, p 221, 1942.
6. E.R. Miller, Medical Physics, Vol. 2, O. Galsser (ed), Year Book Publishers Inc., Chicago, Ill., p 437, 1950.
7. B. Cassen, L. Curtis, C. Reed and R. Libby, Nucleonics, 9:2, p 47, 1951.
8. G.J. Hine and J.J. Erickson, Instrumentation in Nuclear Medicine, Vol. 2, G.J. Hine (ed), Academic Press, New York, 1974.
9. H.O. Anger, Proceedings from a Seminar in Medical Radioisotope Scanning, Vienna, p 59, 1959.
10. H.O. Anger, Donner Lab Semi-annual Report, UCRL-11184, p 69, 1963.
11. H.O. Anger, Rev. Sci. Instr. 29, p 27, 1958.
12. N.F. Moody, W. Paul and M.L.G. Joy, Proc. of the IEEE, 58:2, p 217, 1970.
13. C.A. Tobias, J.H. Lawrence, F.J.W. Roughton, W.S. Root and M.I. Gregersen, Am. J. Physiol. 145, p 253, 1945.
14. F.W. Wren (Jr.), M.L. Good and P. Handler, Science 113, p 525, 1951.
15. G.C. Brownell and W.H. Sweet, Nucleonics 11:11, p 40, 1953.
16. S. Aronow, Instrumentation in Nuclear Medicine, Vol. 1, G.J. Hine (ed), Academic Press, New York, p 461, 1967.

17. H.O. Anger, Nucleonics 21:10, p 56, 1963.
18. H.O. Anger, Instrumentation in Nuclear Medicine, Vol. 1, G.J. Hine (ed), Academic Press, New York, p 486, 1967.
19. G.L. Brownell, C.A. Burnham, B. Hoop (Jr.) and H. Kazemi, Symposium on Medical Radioisotope Scintigraphy, Monte Carlo, Monaco, IAEA/SM-164/158, 1972.
20. G.L. Brownell, Tomographic Imaging in Nuclear Medicine, G.S. Freedman (ed), Society of Nuclear Medicine, New York, 1973.
21. G.N. Hounsfield, Brit. Patent 1,283,915, 1972.
22. H.O. Anger, Instrumentation in Nuclear Medicine,, Vol. 2, G.J. Hine and J.A. Sorenson (ed), Academic Press, New York, p 90, 1974.
23. T.F. Budinger and G.T. Gullberg, Phys. Med. Biol. 19:3, p 387, 1974.
24. Z.H. Cho, I.S. Ahn and C.M. Tsai, IEEE Trans. Nuc. Sci. 21, p 128, 1974.
25. D.A. Chesler, J. Nuc. Med. 12, p 347, 1971.
26. D.A. Chessler, Tomographic Imaging in Nuclear Medicine, G.S. Freedman (ed), Society of Nuclear Medicine, New York, p 176, 1973.
27. M.E. Phelps, E.J. Hoffman, N.A. Mullani and M.M. Ter-Pogossian, J. Nuc. Med. 16:3, p 210, 1975.
28. G.I. Gleason, Int. J. Appl. Rad. 8, p 90, 1960.
29. M.W. Greene and W.O. Tucker, Int. J. Appl. Rad. 12, p 62, 1961.
30. D.K. Beevley, R.J. Post and D.J. Silvester (eds.), Symposium on the use of Cyclotrons in Medicine, MRC Cyclotron Unit, Hammersmith Hospital, London.

31. B. Hoop (Jr. J.S. Laughlin and R.S. Tilbury, Instrumentation in Nuclear Medicine, Vol. 2, G.J. Hine and J.A. Dorenson (ed) Academic Press, New York, p 407, 1974.
32. H.I. Glass, Symposium on Medical Radioisotope Scintigraphy, Monte Carlo, Monaco, IAEA/SM-164/305, 1972.
33. H.I. Glass and D.J. Sylvester, Brit. J. Rad. 43 p 589, 1970.
34. M.S. Livingston and J.P. Blewett, Particle Accelerators, McGraw-Hill Book Co., Inc. Toronto, C p. 3, 1962.
35. R.D. More and J.H. Troughton, Int. J. Appl. Rad. 23, p 344, 1972.
36. A.G. Perris, R.O. Lane, J.Y. Tong and I.D. Matthews, Int. J. Appl. Rad. 25, p 19, 1974.
37. P. Marmier and E.S. Sheldon, Physics of Nuclei and Particles, Vol. 1, Academic Press, Inc. New York, p 519, 1969.
38. J.M. Blatt and V.F. Weiskopf, Theoretical Nuclear Physics, Wiley and Sons, Inc., New York, 1953.
39. R.D. Evans, The Atomic Nucleus, McGraw-Hill Book Co., New York, Chap. 12, Sec. 2, 1955.
40. H.F. Schopper, Weak Interaction and Nuclear Beta Decay, North-Holland Publishing Co., Amsterdam, 1966.
41. C.S. Wu and S.A. Moszkovski, Beta Decay, Interscience Publishers, New York, 1966.
42. C. Strachen, The Theory of Beta Decay, Pergamon Press, Toronto, 1969.
43. S. DeBenedette, C.E. Cowan, W.R. Konneker and H. Primakoff, Phys. Rev. 77, p 205, 1950.
44. B.W. Sargent, Proc. Roy. Soc. (London), A139, p 659, 1933.
45. G. Gamow, Proc. Roy. Soc. (London), A146, p 219, 1934.

47. E.J. Konopinski and G.E. Uhlenbeck, Phys. Rev. 60, p 308, 1941.
48. J.B. Elliot and L. Holm, Machine Procedure Manual, Internal Report, University of Alberta, December, 1969.
49. R. Madey, Engineering Compendium on Radiation Shielding, Vol. 1, Springer-Verlag, Berlin. Sec 2.2.2.1, 1968.
50. E.A. Burris, Engineering Compendium on Radiation Sheilding, Vol. 3, Springer-Verlag, Berlin, Sec 10.7.1.2., 1970.
51. H.W. Patterson and R.H. Thomas, Accelerator Health Physics, Academic Press, New York, 1973.
52. Y.A. Kazanskii, Physics of Reactor Shielding, IPST Press, Jerusalem, 1969.
53. R.G. Jaeger (ed), Engineering Compendium on Radiation Shielding, Vol. 3, Springer-Verlag, Berlin, 1970.
54. D.E. Parks, M.S. Nelkin, J.R. Beyster and N.F. Wikner, Slow Neutron Scattering and Thermalization, W.A. Benjamin, Inc., New York, 1970.
55. S.J. Lindenbaum, Ann. Rev. Nuc. Sci. 2, p 213, 1961.
56. D. Huge and R. Schwartz, Neutron Cross-Sections, BNL-325, 1958.
57. E.A. Burris, Engineering Compendium in Radiation Shielding, Vol. 3, Springer-Verlag, Berlin, Sec 10.7.1.3, 1970.
58. A.G. Perris, R.O. Lane, J.Y. Tong and I.D. Matthews, Int. J. Appl. Rad. 25, p 22, 1974.
59. G.J.F. Legge and I.F. Bubb, Nuc. Phys. 26, p 616, 1961.
60. J.C. Clark and P.D. Buckingham, Int. J. Appl. Rad. 22, p 640, 1971.
61. J.C. Clark and P.D. Buckingham, Int. J. Appl. Rad. 22, p 644, 1971.
62. H.W. Knipping, W. Bolt, H. Valentin, H. Venrath and P. Endler, München. Med. Wochensch. 99, p 46, 1957.

63. H.N. Wagner (Jr.), Dynamic Clinical Studies with Radioisotopes, TID-7678, National Bureau of Standards, Springfield, Virginia, - p 237, 1964.
64. R.S. Jones, T.R. Overton and B.J. Sproule, Amer. Rev. Resp. Dis. (in press).
65. J.B. West, Dynamic Clinical Studies with Radioisotopes, TID-7678, National Bureau of Standards, Springfield, Virginia, p 213, 1964.
66. C.M.E. Matthews, C.T. Dollery, J.C. Clark and J.B. West, Radioactive Pharmaceuticals, CONF 651111, National Bureau of Standards, Springfield, Virginia, p 567, 1966.
67. A.S.E. Fowler, C.M.E. Matthews and E.J.M. Campell, Clinical Sci. 27, p 51, 1964.
68. C.T. Dollery and J.B. West, Proc. Physiol. Soc., July 1960, p 12P, 1960.
69. C.M.E. Matthews, G. Laszlo, E.J.M. Campell, P.M. Kibby and S. Freedman, Resp. Physiol. 6, p 29, 1968/1969.
70. H.B. Jones, Medical Physics, Vol. 2, O. Glasser (ed) Year Book Publishers, Inc., Chicago, Ill., p 855, 1950.
71. N.A. Dyson, P. Hugh-Jones, G.R. Newberry, J.D. Sinclair and J.B. West, Brit. Med. J. 1, p 231, 1960.
72. J.B. West and C.J. Dollery, J. Appl. Physiol. 15, p 411, 1960.
73. C.T. Dollery and J.B. West, Circ. Res. 8, p 765, 1960.
74. C.T. Dollery, N.A. Dyson and J.D. Sinclair, J. Appl. Physiol. 15, p 411, 1960.
75. J. Crofton and A. Douglas, Respiratory Diseases, Blackwell Scientific Publications, New York, 1969.

76. T.R. Overton, L.W. Friedenberg, B.J. Sproule and D. Fenna, Phys. Med. Bio. 18, p 246, 1973.
77. L.W. Friedenberg, M.Sc. Thesis, University of Alberta, 1973.
78. H. Rahn, P. Sadoul, L.E. Farhi and J. Shapiro, J. Appl. Physiol. 8, p 417, 1956.
79. R.U. Corcon and R.J. Robinson, J. Physiol 147, p 469, 1959.
80. A.C. Dryan, L.G. Bentivoglio, F. Beerel, H. MacLeish, A. Zidulka and D.V. Bates, J. Appl. Physiol. 19, p 395, 1964.
81. J.C. Clark and D.J. Sylvester, Int. J. Appl. Rad. 17, p 151, 1966.
82. L. Lindner, T.H.G.A. Suer, G.A. Brinkman and J.T. Veenboer, Int. J. Appl. Rad. 24, p 124, 1973.
83. T. Nozaki, M. Iwamoto and T. Ido, Int. J. Appl. Rad. 25, p 393, 1974.
84. P.V. Harper, N. Lembares and H. Krizek, J. Nuc. Med. 12:6, p 362, 1971.
85. J.S. Fowler, R.D. Finn, R.M. Lambrecht and A.P. Wolf, J. Nuc. Med. 14, p 63, 1973.
86. P.D. Schuman, G. Westmoreland, R. Anderson, "Abstract of Papers, 162nd National Meeting, American Chemical Society", Washington, D.C., Sept., 1971.
87. R.M. Lambrecht, C. Mantescu, J.S. Fowler and A.P. Wolf, J. Nuc. Med. 13:10, p 785, 1972.
88. H.M. Askenasy, M. Anbar, Y. Laor, Z. Lewitus, I.Z. Kosary and S. Guttmann, Am. J. Roent. 88, p 350, 1962.
89. J.J. Kirkland (ed), Modern Practice of Liquid Chromatography, Wiley Interscience, New York, 1971.

90. A.L. Lehninger, A Short Course in Biochemistry, Worth Publishers Inc., New York, p 121, 1973.
91. R. Monks, K.G. Oldham and K.C. Tovey, Labelled Nucleotides in Biochemistry, 12, The Radiochemical Center Ltd., England 1972.
92. N.K. Chaudhuri, B.J. Montag and C. Heidelberger, Can. Res., 18, p 318, 1958.
93. W. Eckhart, Physiol. Rev., 48, p 513, 1968.

B30127